Geosci. Model Dev., 8, 1955–1978, 2015
www.geosci-model-dev.net/8/1955/2015/
doi:10.5194/gmd-8-1955-2015

Geoscientific Model Development
Open Access

^{GA}*SAKe*: forecasting landslide activations by a genetic-algorithms-based hydrological model

O. G. Terranova[1], S. L. Gariano[2,3], P. Iaquinta[1], and G. G. R. Iovine[1]

[1]CNR-IRPI (National Research Council – Research Institute for Geo-Hydrological Protection), via Cavour 6, 87036, Rende, Cosenza, Italy
[2]CNR-IRPI (National Research Council – Research Institute for Geo-Hydrological Protection), via Madonna Alta 126, 06128, Perugia, Italy
[3]University of Perugia, Department of Physics and Geology, via A. Pascoli, 06123, Perugia, Italy

Correspondence to: S. L. Gariano (gariano@irpi.cnr.it)

Received: 12 December 2014 – Published in Geosci. Model Dev. Discuss.: 11 February 2015
Revised: 28 May 2015 – Accepted: 02 June 2015 – Published: 07 July 2015

Abstract. ^{GA}*SAKe* is a new hydrological model aimed at forecasting the triggering of landslides. The model is based on genetic algorithms and allows one to obtain thresholds for the prediction of slope failures using dates of landslide activations and rainfall series. It can be applied to either single landslides or a set of similar slope movements in a homogeneous environment.

Calibration of the model provides families of optimal, discretized solutions (kernels) that maximize the fitness function. Starting from the kernels, the corresponding mobility functions (i.e., the predictive tools) can be obtained through convolution with the rain series. The base time of the kernel is related to the magnitude of the considered slope movement, as well as to the hydro-geological complexity of the site. Generally, shorter base times are expected for shallow slope instabilities compared to larger-scale phenomena. Once validated, the model can be applied to estimate the timing of future landslide activations in the same study area, by employing measured or forecasted rainfall series.

Examples of application of ^{GA}*SAKe* to a medium-size slope movement (the Uncino landslide at San Fili, in Calabria, southern Italy) and to a set of shallow landslides (in the Sorrento Peninsula, Campania, southern Italy) are discussed. In both cases, a successful calibration of the model has been achieved, despite unavoidable uncertainties concerning the dates of occurrence of the slope movements. In particular, for the Sorrento Peninsula case, a fitness of 0.81 has been obtained by calibrating the model against 10 dates of landslide activation; in the Uncino case, a fitness of 1 (i.e., neither missing nor false alarms) has been achieved using five activations. As for temporal validation, the experiments performed by considering further dates of activation have also proved satisfactory.

In view of early-warning applications for civil protection, the capability of the model to simulate the occurrences of the Uncino landslide has been tested by means of a progressive, self-adaptive procedure. Finally, a sensitivity analysis has been performed by taking into account the main parameters of the model.

The obtained results are quite promising, given the high performance of the model against different types of slope instabilities characterized by several historical activations. Nevertheless, further refinements are still needed for application to landslide risk mitigation within early-warning and decision-support systems.

1 Introduction

A nationwide investigation, carried out by the National Geological Survey, identified approximately 5×10^5 slope movements in Italy, with an average of 1.6 failures per square kilometer (Trigila, 2007). According to other investigations, this figure would rather be a low estimate (cf. Servizio Geologico, Sismico dei Suoli, 1999; Guzzetti et al., 2008). In the period 1950–2009, at least 6349 persons were killed, went missing, or were injured by landslides, with an average of 16 harmful

events per year, thus confirming the notable risk posed to the population (Guzzetti, 2000; Salvati et al., 2010).

Petley (2008) estimated that about 90 % of worldwide casualties can be attributed to landslides triggered by rainfall. With reference to the Italian territory, about 70 % of landslides result from being triggered by rainfall (cf. CNR-GNDCI AVI Project, Alfieri et al., 2012). Slope instability conditions are in fact influenced by rainfall that, infiltrating into the slopes, causes temporary changes in groundwater dynamics (Van Asch et al., 1999). The combination of infiltration and runoff may cause different types of mass movements (either slope failure or erosion processes) depending on the intensity and duration of the rainfall and the values of soil suction (Cuomo and Della Sala, 2013). Concentration of water deriving from either contemporary or antecedent storms at specific sites plays a major role in triggering landslides – as testified by slope instabilities that commonly follow the heaviest phases of rainfall events.

To model the relationships between rainfall and landslide occurrence, two distinct approaches are generally adopted in the literature. The first, named "complete" or "physically based", attempts to determine the influence of rainfall on slope stability by modeling its effects in terms of overland flow, groundwater infiltration, pore pressure and related balance of shear stress and resistance (cf. e.g., Montgomery and Dietrich, 1994; Wilson and Wieczorek, 1995; Crosta, 1998; Terlien, 1998; Crosta et al., 2003; Pisani et al., 2010). With regard to this latter purpose, numerical models are employed, and a notable (and expensive) number of detailed data are commonly required to define the geological scheme of the slope in litho-structural, hydrogeological, morphologic and geotechnical terms. The second approach (adopted in the present study), named "empirical" or "hydrological" (Cascini and Versace, 1988), is based on a statistical–probabilistic analysis of rainfall series and of dates of occurrence of slope movements (see, among others, Campbell, 1975; Caine, 1980; UNDRO, 1991; Sirangelo and Versace, 1996; Guzzetti et al., 2007, 2008, Brunetti et al., 2010; Gariano et al., 2015). In the literature, methodological examples generally focus on thresholds obtained for (i) single phenomena or (ii) given types of landslides within a homogeneous geo-environmental setting (cf. e.g., Jakob and Weatherly, 2003).

In this study, hydrological model ^{GA}*SAKe* (i.e., the genetic-algorithms-based release of the **S**elf **A**daptive **Ke**rnel) model, developed to forecast the triggering of slope movements, is described. The model can be applied to either single landslides or to a set of similar phenomena within a homogeneous study area. Model calibration is performed by means of genetic algorithms: in this way, a family of optimal, discretized kernels can iteratively be obtained from initial tentative solutions. In a different release of the model (^{CM}*SAKe* – i.e., *cluster model SAKe*), the calibration is instead performed through an iterative procedure (Terranova et al., 2013).

Examples of application of the model to a medium-size landslide (the Uncino landslide at San Fili) and to shallow-slope movements in the Sorrento Peninsula are discussed in the following sections. Temporal validation is discussed for both cases, in view of early-warning applications of ^{GA}*SAKe* for civil protection purposes. Moreover, a progressive, self-adaptive procedure of calibration and validation is discussed, by considering the Uncino case study, to verify changes in fitness, predictive ability and base time when an increasing number of dates of activation is employed. Finally, the results of preliminary parametric analyses are presented, aimed at investigating the role of the main parameters of the model.

2 Background

Physical systems evolve in time due to their own inner dynamics and/or as a consequence of external causes. Suitable observational tools can be employed to monitor their evolution, and arranged to promptly send reports or warnings to authorities of civil protection to support the management of emergencies (Cauvin et al., 1998; for applications to landslides, cf. also Keefer et al., 1987; Iovine et al., 2009; Capparelli and Versace, 2011; Pradhan and Buchroithner, 2012).

In the case of complex systems (e.g., nuclear power stations, telecommunication networks), many parameters, in part interdependent, have to be monitored. Missing an automated phase of analysis and proper filtering, a great number of reports may be delivered by the monitoring apparatus in a few seconds. For this purpose, the concepts of threshold (Carter, 2010), event and warning must therefore be suitably defined.

Regarding slope movements, the notions of threshold and warning have long been investigated. In particular, a threshold constitutes a condition – generally expressed in quantitative terms or through a mathematical law – whose occurrence implies a change of state (White et al., 1996). According to the ALARM study group (Cauvin et al., 1998), an event is (i) a portion of information extracted from either continuous or discrete signals (i.e., a significant variation), transmitted by a component of the monitoring network; or (ii) a set of data concerning the considered context (e.g., restorations, actions, observations). According to such a definition, an event must be instantaneous and dated. As for warning, its definition derives from that of the event: it is a discrete indicator aimed at triggering a human or an automated reaction. The warning can be classified into distinct levels (e.g., in terms of security) or by type (e.g., related to a distinct component of the dynamic system under consideration), to be transmitted by the monitoring system.

In complex systems, causal factors responsible for emergency conditions may be difficult to identify. Therefore, warnings may be issued according to pre-fixed thresholds related to suitable physical properties of the system. In these cases, the timing of data sampling of the monitoring instru-

ments should be progressively adapted to the evolution of the phenomenon. A further issue concerns the chances of missing and false alarms, as well as the camouflage of an alarm among simultaneous others.

In physical terms, slope instability can occur when the shear strength gets lower than a given threshold (Terzaghi, 1962). Rain infiltration may temporarily change the dynamics of groundwater (Van Asch et al., 1999): due to an increase in pore water pressure, the effective shear strength of the material decreases, and a slope movement can be triggered. Groundwater may reach a given location within the slope by different paths. The main natural mechanisms include (i) surface flow, strongly influenced by morphology; (ii) direct infiltration from the surface; (iii) flow within the soil mantle (*throughflow*) from upslope and sideslopes; and (iv) seepage from the bedrock toward the overlying colluvium. The length of the different paths may be quite different, and is characterized by distinct velocities: as a consequence, aliquots of the same rainfall event may reach a given site at different times, variously combining with other groundwater amounts (Ellen, 1988).

To apply a hydrological approach, empirical relations have to be determined by means of thresholds to distinguish among conditions that likely correspond to landslide occurrence or not. To this aim, different hydrological parameters can be selected (Guzzetti et al., 2007, 2008, and http://rainfallthresholds.irpi.cnr.it/): the cumulative rain recorded in a given temporal window (hours/days/months) before landslide activation; the average rain intensity in the same temporal window; and rains normalized to reference values (e.g., annual averages). Simplified hydrological balances can also be adopted in empirical approaches, by considering losses of aliquots of rains by runoff, evapo-transpiration, etc.

Regarding superficial landslides, triggering thresholds can be derived from relations between the "triggering" rain (daily, hourly or shorter), corresponding to the onset of the slope movement, and the rain cumulated over an "antecedent period" (usually, a few days to 2 weeks before landslide activation) (e.g., Campbell, 1975; Cannon and Ellen, 1985; Wieczorek, 1987; Terlien, 1996; Crosta, 1998; Zêzere and Rodrigues, 2002). In other cases, thresholds refer to relations between rain intensity, I, and duration, D (e.g., Brunetti et al., 2010; Berti et al., 2012; Peres and Cancelliere, 2014). In some studies, antecedent rains are also considered, allowing one to obtain better results (e.g., Campbell, 1975). Larger amounts of antecedent rain should allow slope movements to be activated by less severe triggering storms. In general, a direct relationship between antecedent rain and landslide dimension can be observed (Cascini and Versace, 1986), though, under some peculiar conditions (e.g., Hong Kong case studies, caused by suction reduction – Brand et al., 1984), this is not the case, and the role of antecedent rains looks less important. In addition, as underlined by Cuomo and Della Sala (2013), time to runoff, time to failure and runoff rates strongly depend on soil water characteristic curves, soil initial conditions, rainfall intensity and slope angle in unsaturated shallow deposits. Moreover, soil mechanical parameters affect the time to failure, which can be either shorter or longer than time to runoff.

Due to physical and economic issues, difficulties in hydrological modeling of landslides generally increase when dealing with deeper and larger phenomena (Cascini and Versace, 1986). In such cases, landslide activation depends on the dynamics of deeper groundwater bodies. By the way, it is not by chance that most studies do refer to small and superficial slope movements. Large landslides usually show complex relationships with rains, as different groundwater aliquots may combine and reach the site of triggering. Depending on type (cf. dimension, material, kinematics, etc.), different hydrological mechanisms should be considered, thus limiting the possibility of generalization of the thresholds (Dikau and Schrott, 1999; Corominas, 2001; Marques et al., 2008). Again, the mobilization of deeper phenomena commonly requires greater rainfall amounts, spanned over longer periods, with respect to shallow landslides (Aleotti, 2004; Terranova et al., 2004; Guzzetti et al., 2007, 2008). In these cases, rain durations responsible for landslide activations commonly range from ca. 30 days to several months, even beyond a single rainy season (Brunsden, 1984; Van Asch et al., 1999; Gullà et al., 2004; Trigo et al., 2005).

To analyze the triggering conditions of slope movements – either shallow or deep-seated – a threshold-based modeling approach can be employed. Empirical thresholds (e.g., Aleotti, 2004; Wieczorek and Glade, 2005; Terranova et al., 2004; Vennari et al., 2014) can be expressed in terms of curves, delimiting the portion of the Cartesian plane that contains "all and only" the hydrological conditions related to known activations (cf. e.g., the I–D chart proposed by Caine, 1980). A further improvement to this approach can be obtained by considering hydrological conditions not related to landslide activations (Crozier, 1997; Sengupta et al., 2010; Gariano et al., 2015). In general, no changes of state are assumed to occur below the threshold (z_t), while they do happen above it. Alternatively, a range of conditions can be defined (Crozier, 1997), delimited by

- a lower threshold (z_{low}), below which changes of state never occur, and
- an upper threshold (z_{upp}), above which changes always happen.

For values between z_{upp} and z_{low}, the probability that the state changes can be defined, essentially depending on (i) the incompleteness of knowledge of the physical process under investigation, and (ii) the incapacity of the model to fully replicate the behavior of the same process. In probabilistic terms,

$$P(E_t) = 0 \text{ for } z(t) < z_{\text{low}},$$
$$P(E_t) = 1 \text{ for } z(t) > z_{\text{upp}},$$
$$P(E_t) = G[z(t)] \text{ for } z_{\text{low}} \le z(t) \le z_{\text{upp}}, \quad (1)$$

in which P is the probability of occurrence (1 = success, 0 = unsuccess); E_t is a process (succession of events) whose state changes with time t; $z(t)$ is the value assumed, at time t, by the variable that determines the change of state; z_{low} and z_{upp} are the minimum and maximum thresholds, respectively; and $G[z(t)]$ is a probability function, monotonically increasing with t in the range $]0, 1[$.

In hydrological models, to express the influence of rainfall on runoff and groundwater dynamics, a "kernel" (also named a "filter function") can be employed, usually defined in terms of a simple, continuous analytical function (Chow et al., 1988). In such a way, suitable weights can be assigned to the precipitations that occurred in the last hours/days before a given geo-hydrological process (e.g., discharge, measured at a generic river cross section, landslide activation), as well as to earlier rains recorded weeks/months before. The most employed types of kernels are beta, gamma, Nash, and negative exponential distribution. Furthermore, the "base time" (t_b) expresses a sort of memory with respect to rainfall: in classic rainfall–runoff modeling, t_b defines the time of concentration, while in slope stability analyses, it represents the time interval, measured backward from landslide activation, during which rainfall is deemed to effectively affect groundwater dynamics, and contributes to destabilization.

To model slope stability, both the shape and the base time of the kernel must be properly selected depending on the type and dimension of the investigated phenomena, as well as geo-structural and hydrogeological characteristics. Unfortunately, in several real cases, the abovementioned analytical functions may fail in properly capturing the complexity of groundwater dynamics, as well as the related landslide activations. In this respect, the adoption of discretized kernels, automatically calibrated through iterative computational techniques, may offer effective solutions.

3 The GA*SAKe* model

GA*SAKe* is an empirical–hydrological model for predicting the activation of slope movements of different types. It is based on a classic threshold scheme: the exceedance of the threshold determines a change of state, i.e., the triggering of the landslide. The scheme is inspired by the *FLaIR* (**F**orecasting **La**ndslides **I**nduced by **R**ainfall) model, proposed by Sirangelo and Versace (1996): through changes of state in time, the variable $z(t)$ assumes the meaning of a "mobility function". In other terms, the values of $z(t)$ depend on the amount of rain stored in the aquifer.

In hydrology, rainfall–runoff modeling is commonly performed by adopting a linear, steady scheme (Chow et al., 1988). Such an approach implies that the transformation of rainfall in runoff can be described by an integral of convolution between a unitary impulsive response of the basin – the kernel, $h(t)$ – and the rainfall, $p(t)$.

The *kernel* (*filter function*) represents the unitary volume influx in an infinitesimal period, and is defined as

$$\int_0^\infty h(t)\,\mathrm{d}t = 1, \quad (2)$$

in which $h(t) = h(-t)$, $h(t) \ge 0$, $\forall t$.

In practical applications, the lower bound ($t = 0$) corresponds to the beginning of the flood-wave rising, and the kernel assumes a finite duration (t_b). The integral of convolution is therefore expressed as

$$z(t) = \int_0^{t_b} h(t-\tau)\; p(\tau)\,\mathrm{d}\tau = \int_0^{t_b} h(\tau)\; p(t-\tau)\,\mathrm{d}\tau, \quad (3)$$

in which $z(t)$ represents the discharge at time t. For a specific case study, the kernel can be determined by means of calibration procedures, by relating discharge measurements to rains.

In discretized terms, the elements of the kernel are characterized by width Δt and height h_i, and Eq. (3) can be written as

$$z_u = \sum_{i=1}^{u} h_i \cdot p_{u-i+1} \cdot \Delta t. \quad (4)$$

Sirangelo and Versace (1996) proved that the same approach may turn out to be promising also in slope-stability modeling. Capparelli and Versace (2011) stressed that the I–D chart of Caine (1980) corresponds to a kernel defined by a power function $h(t) = a\,t^b$, with $b < 0$. Exporting the well-established knowledge of rainfall–runoff modeling (usually based on many measurements) to rainfall–landslide modeling is not trivial, due to the scarcity of adequate information for proper calibration. Only a few dates of activation are, in fact, commonly available in rainfall–landslide modeling (often with unsatisfactory details on location and phenomena), and the values of $z(t)$ are unknown. From a mathematical point of view, such a problem can be handled by assuming that the timing of the maxima of $z(t)$ corresponds to the dates of landslide activation. When studying the triggering conditions of landslides, calibration can therefore be performed by maximizing the mobility function in correspondence to the dates of activation.

Scarcity of information inevitably reflects on the resulting kernel, whose shape may turn out highly indeterminate: different functions, or different parameters of the same function, can in fact maximize $z(t)$ in correspondence to the dates of mobilization. Model optimization – and its reliable utilization for early-warning purposes – can turn out to be an awkward issue.

In this work, an innovative modeling approach – based on discretized kernels, automatically calibrated through iterative computational techniques – is proposed, which may help in facing the above-cited difficulties. For modeling purposes, the rainfall series and a coherent set of dates of landslide occurrence – either related to a given slope movement, or to a set of landslides of the same type in a homogeneous geo-environmental zone – must be given as input.

Unfortunately, when dealing with the timing of occurrence, historical notices may refer either to portions of the considered phenomena or to entire landslide bodies. Therefore, dates should be properly selected to consider only consistent cases. Moreover, dates of activation are usually known with only a broad approximation: with respect to the reports, the actual timing of occurrence may be located backward (documents may assign a later date) or forward (in the case of later, more relevant movements). For modeling purposes, it is then useful to specify a temporal window, lasting from an initial ($d_{t-\mathrm{from}}$) to a final date ($d_{t-\mathrm{to}}$), containing the presumable timing of occurrence.

Rainfall series are commonly reconstructed from data recorded at rain gauges located within a reasonable proximity of the study site. The temporal window of the hydrological analysis is defined by the intersection of (i) the period of observation of the rains and (ii) the period delimited by the most ancient and most recent dates of activation of the landslide. A potential source of uncertainty lies in the fact that, occasionally, the recorded rainfall amounts notably differ from those actually experienced at landslide location. Furthermore, landslide triggering may also be due to other causes (e.g., human activity, earthquakes): a thorough preliminary analysis has always to be performed to verify the significance of rainfall preceding landslide activation, to detect cases not to be considered in the hydrological study.

In the model, rains older than t_{b} are neglected. Suitable maximum and minimum values ($t_{\mathrm{b\text{-}max}}$ and $t_{\mathrm{b\text{-}min}}$) have to be initialized to allow the model to determine optimal values. Commonly, t_{b} ranging from a few hours to some weeks are suggested for shallow landslides, while greater values (up to several months) sound suitable for deep-seated phenomena.

Based on the geological knowledge of the phenomenon under investigation, the initial shape of the kernel can be assumed among a set of basic types. Among these, (i) a "rectangular" shape can be adopted if older precipitations have the same weight of more recent rains; (ii) a "decreasing triangular", if older precipitations have a progressively smaller weight than more recent rains; and (iii) "increasing triangular", if older precipitations have a progressively greater weight than more recent rains. A casual shape or any other function can also be implemented in the model (e.g., beta, gamma, Nash, negative exponential distribution).

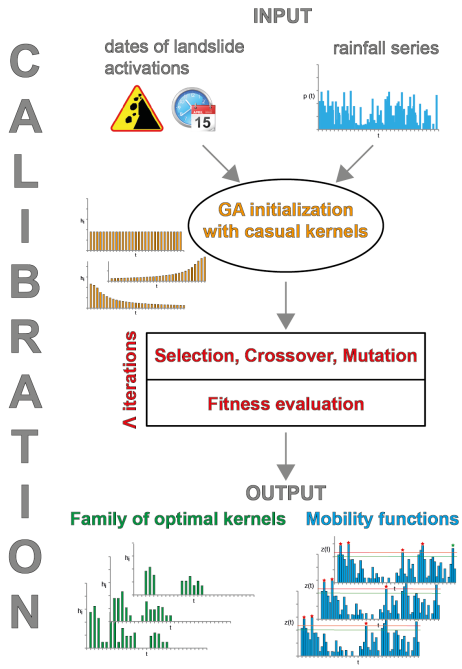

Figure 1. Scheme of the calibration procedure of the GA*SAKe* model.

3.1 Model calibration

In GA*SAKe*, model calibration is performed against real case studies through genetic algorithms (GAs). These latter ones are general-purpose, iterative search algorithms inspired by natural selection and genetics (Holland, 1975). Since the 1970s, GAs have been applied to several fields of research, from applied mathematics (Poon and Sparks, 1992), to evolution of learning (Hinton and Nowlan, 1987), evolutionary robotics (Nolfi and Marocco, 2001), and debris-flow modeling (Iovine et al., 2005; D'Ambrosio et al., 2006). GAs simulate the evolution of a population of candidate solutions to a given problem by favoring the reproduction of the best individuals. The candidate solutions are codified by genotypes, typically using strings, whose elements are called genes.

GAs explore the solution space, defined as the set of possible values of the genes. At the beginning of a given optimization experiment, the members of the initial population of genotypes (in this study, the *kernels*) are usually generated at random. The performance of each solution, in terms of phenotype (i.e., the *mobility function*), is evaluated by applying a suitable *fitness function*, thus determining its "adaptability", i.e., the measure of its goodness in resolving the problem.

The sequence of random genetic operators *selection*, *crossover* and *mutation*, constrained by prefixed probabilities, constitutes a single GA iteration that generates a new population of candidate solutions. At each iteration, the best individuals are in fact chosen by applying the selection operator. To form a new population of offspring, crossover is

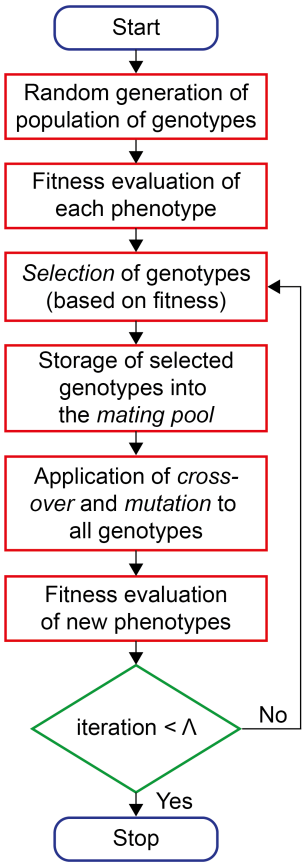

Figure 2. Scheme of the adopted genetic algorithm.

employed by combining parents' genes. Mutation is successively applied to each gene, by randomly changing its value within the allowed range. Thanks to the GA approach, better individuals (i.e., those characterized by higher fitness values) can be obtained over time. In fact, according to individual probabilities of selection, any change that increases the fitness tends to be preserved over GA iterations (Holland, 1975). For further details on GAs, cf. Goldberg (1989) and Mitchell (1996).

In the present study, a steady-state and elitist GA (cf. De Jong, 1975) was employed to obtain the family of optimal kernels that maximize the mobility function in correspondence to known dates of landslide activations. The procedure employed for calibration of GA*SAKe* is schematized in Fig. 1.

At the beginning of an optimization experiment, the initial population of N kernels is generated at random, and the fitness of the related mobility functions is evaluated (cf. below). In order to evolve the initial population of candidate solutions, and to progressively obtain better solutions, a total number of Λ GA iterations follow.

At each iteration of the GA, the operator selection, crossover and mutation are applied as follows (Fig. 2):

– *selection*

  i. n_e "elitist" individuals are merely copied in a "mating pool" from the previous generation, by choosing the best ones; and

  ii. the remaining $N - n_e$ candidate solutions are chosen by applying the "tournament without replacement" selection operator. More in detail, a series of tournaments are performed by selecting two individuals at random from the previous generation: the winner (i.e., the one characterized by the highest fitness) is copied into the mating pool, according to a prefixed surviving probability (p_s), which is set greater for the fittest individual. Note that, when choosing the $N - n_e$ candidate solutions, a given individual cannot be selected more than once.

– *crossover*

After the mating pool is filled with N individuals, the crossover operator is applied, according to a prefixed probability (p_c):

  i. two parent individuals are chosen from the mating pool at random;

  ii. a cutting point (*crossover point*) is then selected at random in the range $]t_{b\text{-}min}, t_{b\text{-}max}[$;

  iii. the obtained portions of parents' strings are exchanged, thus mixing the genetic information and resulting in two children (Fig. 3).

When the crossover is not applied, the two parents are merely copied into P_{new}.

– *mutation*

Based on a prefixed probability (p_m), a random number of elements of the kernel (p_{me}, expressed as a percentage of t_b) is mutated, by adding to each element an amount dh that is randomly obtained in the range $[p_{mh1}, p_{mh2}]$, as a function of the maximum value of the kernel (h_{max}). Then dh ranges from dh_1 to dh_2:

$$\begin{aligned} \mathrm{d}h_1 &= p_{mh1} \cdot h_{max} \\ \mathrm{d}h_2 &= p_{mh2} \cdot h_{max}. \end{aligned} \quad (5)$$

Furthermore, the base time is also mutated (increased or decreased) within the bounds $[t_{b\text{-}min}, t_{b\text{-}max}]$, according to a random factor dt_b selected in the range $[1/p_{mtb}, p_{mtb}]$ (Fig. 4).

Children obtained by either crossover or mutation must be normalized before being included in the population P_{new}, by properly scaling the elements of the kernels to ensure the validity of Eq. (2).

During calibration, the shape of the kernel and its t_b are iteratively refined. Note that the shape is not subject to any constraint, while t_b is allowed to vary in the range $[t_{b\text{-}min} - t_{b\text{-}max}]$. The fitness is computed for each examined mobility

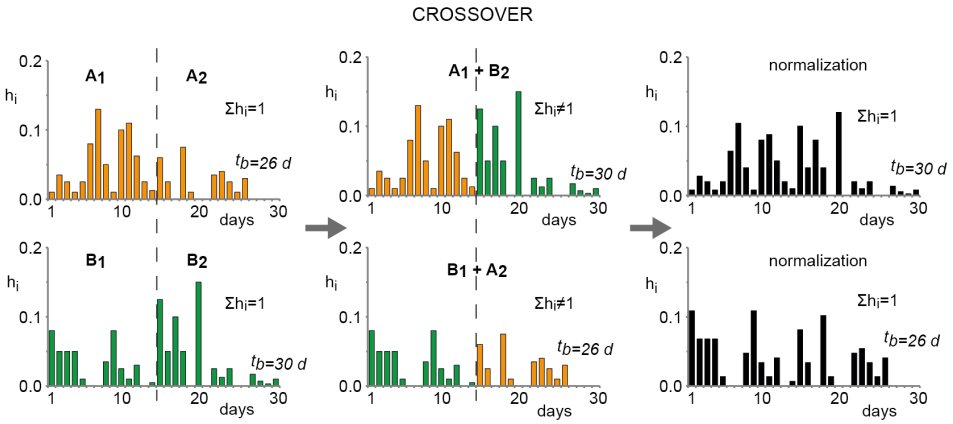

Figure 3. Example of crossover. The genetic codes of the parents (elements in orange and green) are first mixed; then, the children are normalized (black elements) to ensure the validity of Eq. (2).

function, and new populations of kernels are generated as described above.

As for the fitness function, in GA*SAKe* it is defined as follows:

- the L available dates of landslide activation – as derived from the historical analyses – are arranged in a vector $\boldsymbol{S} = \{S_1, S_2, \ldots, S_i, \ldots, S_L\}$;
- the vector of the relative maxima of the mobility function, $\boldsymbol{Z} = \{z_1, z_2, \ldots, z_j, \ldots, z_M\}$, is sorted in decreasing order (M = number of relative maxima); and
- the vector of the partial fitness is $\boldsymbol{\varphi} = \{\varphi_1, \varphi_2, \ldots, \varphi_i, \ldots \varphi_L\}$, where $\varphi_i = k^{-1}$ depends on the rank k of the relative maxima of z_j that coincide with known dates of activation, S_i. In case S_i does not correspond to any relative maximum, it is $\varphi_i = 0$.

With reference to a given kernel, the resulting fitness is expressed by $\Phi_u = \sum_{i=1}^{L} \varphi_i$. To generalize the results for an easier comparison with other study cases, a normalized fitness index is adopted, $\Phi = \Phi_u / \Phi_{\max}$, defined in the range [0,1], being $\Phi_{\max} = \sum_{i=1}^{L} 1/i$.

For instance, if two dates of activation are available and both are well captured by the mobility function (i.e., they correspond to the highest peaks), the obtained fitness is $\Phi_u = 1+1/2 = 1.5$. On the other hand, in case only one of the dates is captured and the remaining one ranks fifth, $\Phi_u = 1+1/5 = 1.2$.

Thanks to the above procedure, a family of "optimal kernels" that maximizes the fitness can be determined. The mobility function is, in fact, forced toward a shape characterized by relative maxima (z_j) coinciding with the dates of landslide occurrence (S_i). An optimal solution leads to a mobility function having the highest peaks in correspondence to such dates; further peaks may also be present, characterized by lower values. Nevertheless, kernel solutions generally determine mobility functions whose highest peaks only partly match the dates of landslide occurrence (i.e., some dates may neither correspond to the highest peaks nor to any peak at all).

To select the most suitable kernel from a given family of optimal ones, let us define

- $z_{j-\min}$ as the lowest of the peaks of the mobility function in correspondence to one of the dates of activation (S_i);
- $z_{\rm cr}$ as the "critical threshold", i.e., the highest peak of the mobility function just below $z_{j-\min}$; and
- the "safety margin", $\Delta z_{\rm cr} = (z_{j-\min} - z_{\rm cr})/z_{j-\min}$.

When applying the fitness function to evaluate a given kernel, either incompleteness or low accuracy of input data may lead to "false alarms" – i.e., peaks of the mobility function (z_j) that are greater than the threshold $z_{\rm cr}$, but that do not correspond to any of the known dates of activation. Such alarms can actually be of two different types: (1) "untrue false", due to an informative gap in the archive (i.e., correct prediction); and (2) "true false", in the case of real misprediction of the model. In such cases, further historical investigations may help to discriminate between the mentioned types of false alarms.

Also depending on the specific purpose of the analysis, the most suitable kernel can therefore be selected by one or more of the following criteria: (i) the greatest $\Delta z_{\rm cr}$; (ii) the shortest $t_{\rm b}$; and (iii) the smallest $\mu_0 = \sum_{i \le t_{\rm b}} (i - 0.5)\, h_i\, \Delta t$, i.e., the first-order momentum of the kernel with respect to the vertical axis. The first criterion allows for the activation of early-warning procedures with the greatest advance; the remaining ones (to be employed when $\Delta z_{\rm cr}$ is too small) generally correspond to more impulsive responses to rainfall.

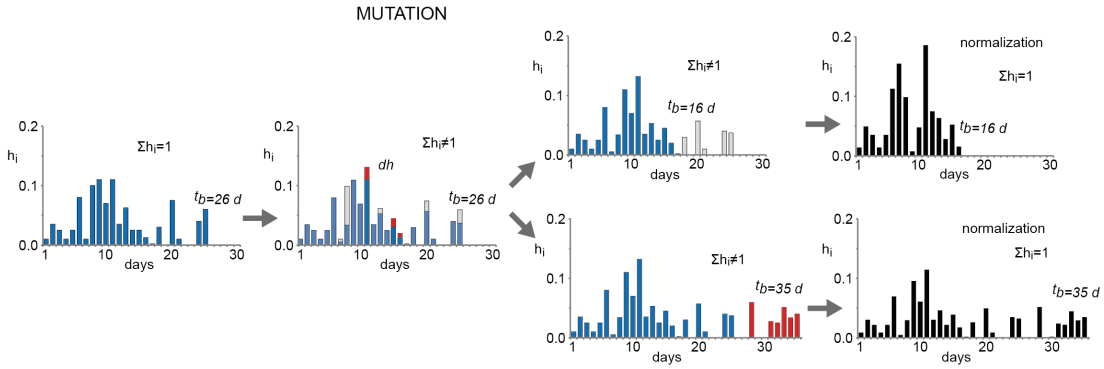

Figure 4. Examples of mutation. On the left, the genetic code of the parent individual (elements in blue). In the second histogram, mutation is applied to some elements of the parent (in red, added amounts; in grey, subtracted amounts). Then, the base time can either be decreased (upper sequence) or increased (lower sequence). Finally, the children are normalized (black elements) to ensure the validity of Eq. (2).

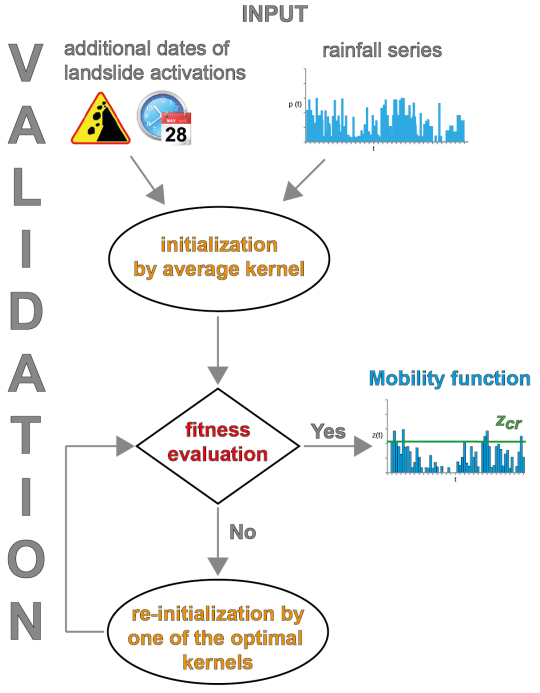

Figure 5. Scheme of the validation procedure of the GA*SAKe* model.

Differently from what is usually experienced in rainfall–runoff models, GA*SAKe* therefore provides multiple equivalent solutions – i.e., a number of optimal kernels with same fitness, Φ_u, despite different shapes. This may depend on the limited number of available dates of activations, and on other noises in input data (e.g., rain gauges located too far from the site of landslide activation, inaccurate information on dates of activation or on the phenomenon). The adoption of synthetic kernels – e.g., obtained by averaging a suitable set of optimal kernels – permits one to synthesize the family of results for successive practical applications: in this work, the 100 best kernels obtained for each case study were in fact utilized to synthesize "average kernels" (see below) to be employed for validation purposes.

4 Case studies

The case studies considered in this paper are (i) a set of shallow landslides in the Sorrento Peninsula between Gragnano and Castellammare di Stabia (Campania, southern Italy) and (ii) the Uncino landslide at San Fili (Calabria, southern Italy).

Note that, as the numbers of known historical activations in the study areas were adequate, some dates could be excluded from calibration, and were successively employed for validation purposes. In particular, the most recent dates of landslide activation (cf. Tables 1 and 2) were employed to validate the average kernels (these latter ones obtained from the families of optimal solutions defined through calibration). The procedure employed for validation is schematized in Fig. 5.

4.1 Shallow landslides in the Sorrento Peninsula – Campania

The Sorrento Peninsula is located in western Campania, southern Italy (Fig. 6). In the area, Mesozoic limestone mainly crops out, covered by Miocene flysch, Pleistocene volcanic deposits (pyroclastic fall, ignimbrite), and Pleistocene detrital–alluvional deposits (Di Crescenzo and Santo, 1999). The carbonate bedrock constitutes a monocline, gently dipping towards WNW, mantled by sedimentary and volcanoclastic deposits, with thicknesses ranging from a few decimeters to tens of meters.

Rainfall-induced shallow landslides are widespread in the pyroclastic soils covering the slopes of the study area. Among the various factors affecting the spatial distribution and the type of slope instabilities, Cascini et al. (2014) pointed out that both the rainfall conditions and the conse-

Table 1. Dates of activation of the shallow landslides in the Sorrento Peninsula. Key: date: day of occurrence; type: widespread (multiple) or few (single) activation; site: municipality including the affected location; period employed: dates used for calibration (except for no. 11); rank: relative position of the corresponding maximum of the mobility function obtained by calibration. An asterisk marks the date employed for validation. In italics, the activation date (no. 0) excluded due to hydrological constraints.

No.	Date	Type	Site	Reference	Period employed	Rank
1	17 Feb 1963	Multiple; single	Gragnano, Pimonte; Castellammare	Del Prete et al. (1998)	17 Feb 1963	17 Feb 1963 (1)
2	23 Nov 1966	Single	Vico Equense (Scrajo), Arola, Ticciano	Del Prete et al. (1998)	23 Nov 1966	24 Nov 1966 (4)
0	*14 Apr 1967*	*Single*	*Castellammare (Pozzano)*	*Del Prete et al. (1998); AMRA (2012)*	–	–
3	15 Mar 1969; 24 Mar 1969	Multiple; multiple	Cava de' Tirreni, Agerola, Scrajo Seiano	Del Prete et al. (1998); AMRA (2012)	15–24 Mar 1969	25 Mar 1969 (65)
4	02 Jan 1971	Single	Gragnano	Del Prete et al. (1998)	02 Jan 1971	03 Jan 1971 (3)
5	21 Jan 1971	Single	Gragnano	Del Prete et al. (1998)	21 Jan 1971	21 Jan 1971 (7)
6	04 Nov 1980	Single	Vico Equense (Scrajo)	Del Prete et al. (1998)	04 Nov 1980	06 Nov 1980 (94)
7	14 Nov 1982	Single	Pozzano	Del Prete et al. (1998)	14 Nov 1982	15 Nov 1982 (151)
8	22 Feb 1986	Multiple	Palma Campania, Castellammare, Vico Equense	Del Prete et al. (1998)	22 Feb 1986	24 Feb 1986 (120)
9	23 Feb 1987	Single	Gragnano, Castellammare	Del Prete et al. (1998); AMRA (2012)	23 Feb 1987	23 Feb 1987 (73)
10	23 Nov 1991	Single	Pozzano	Del Prete et al. (1998)	23 Nov 1991	24 Nov 1991 (43)
11	10 Jan 1997	Multiple	Pozzano; Castellammare, Nocera, Pagani, Amalfitana Coast	Del Prete et al. (1998); AMRA (2012)	10 Jan 1997	*

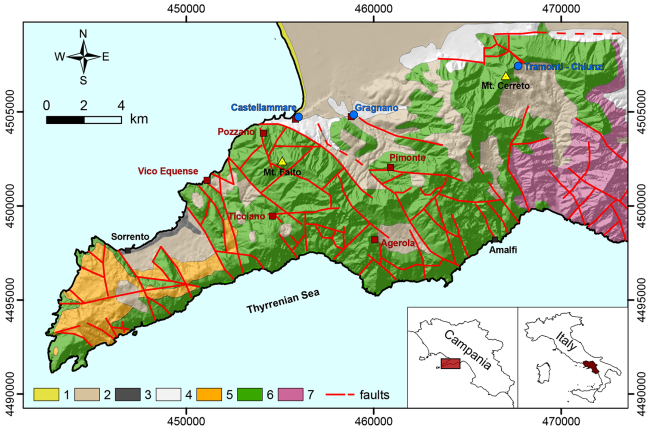

Figure 6. Geological map of the Sorrento Peninsula (after Di Crescenzo and Santo, 1999, mod.). Key: (1) beach deposit (Holocene); (2) pyroclastic fall deposit (late Pleistocene–Holocene); (3) Campanian ignimbrite (late Pleistocene); (4) detrital alluvial deposit (Pleistocene); (5) flysch deposit (Miocene); (6) limestone (Mesozoic); (7) dolomitic limestone (Mesozoic). Red squares mark sites affected by shallow landslide activations; blue circles, the rain gauges; black squares, the main localities; yellow triangles, the highest mountain peaks.

quent seasonal variations of soil suction play a significant role. In particular, when suction is low and frontal rainfall occurs (from November to May), first time shallow landslides are triggered; when suction is high or very high and convective or hurricane-type rainfall occurs (from June to October), mostly erosion phenomena occur, often turning into hyperconcentrated flows.

The study area is characterized by hot, dry summers and moderately cold and rainy winters. Consequently, its climate can be classified as Mediterranean (Csa in the Köppen–Geiger classification). In particular, the mean annual temperature ranges from 8–9 °C, at the highest elevations of M. Faito and M. Cerreto, to 17–18 °C along coasts and valleys. Average annual rainfall varies from 900 mm west of Sorrento to 1500 mm at M. Faito; moving inland to the east, it reaches 1600 mm at M. Cerreto and 1700 mm at the Chiunzi pass (Ducci and Tranfaglia, 2005). On average, annual totals are concentrated on about 95 rainy days. During the driest 6 months (from April to September), only 30 % of the annual rainfall is recorded in about 30 rainy days. During the three wettest months (November, October, and December), a similar amount is recorded in about 34 rainy days (Servizio Idrografico, 1948–1999). In the area, convective rainstorms may occur, characterized by a very high intensity, at the beginning of the rainy season (from September to October). In autumn–winter, either high intensity or long duration rainfall are usually recorded, while uniformly distributed rains generally occur in spring (Fiorillo and Wilson, 2004). As for annual maxima of daily rainfall recorded at sea level, the Amalfi coast (southern border of the Sorrento Peninsula) is characterized by smaller values (59 mm) of average annual maxima of daily rainfall than the Sorrento coast (86 mm), on the northern border. Such a difference seems to persist even at higher elevations (up to 1000 m a.s.l.), with 84 mm vs. 116 mm for the southern and northern mountain slopes, respectively (Rossi and Villani, 1994).

Severe storms frequently affect the study area, triggering shallow landslides that propagate seaward, often causing casualties and serious damage to urbanized areas and trans-

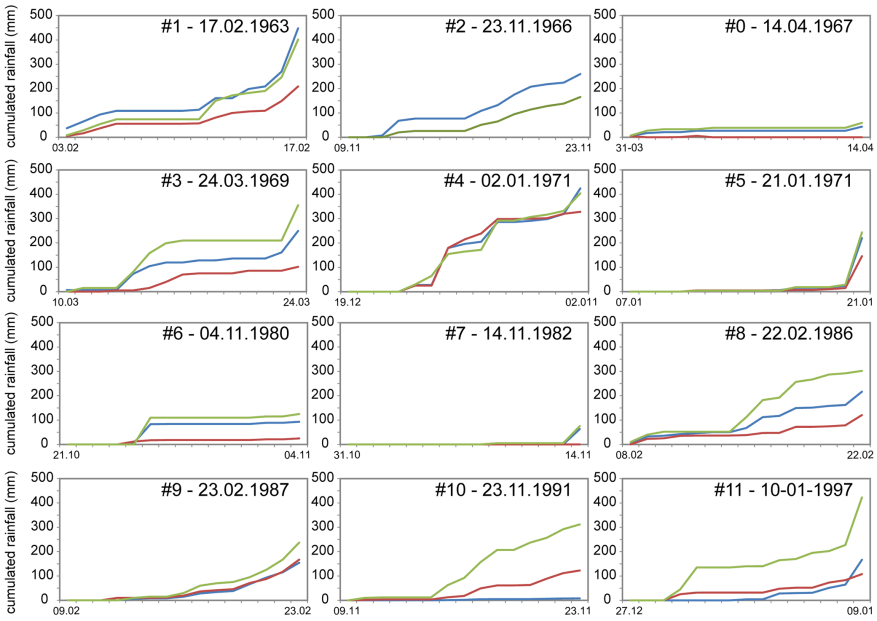

Figure 7. Cumulative daily rainfall (in mm) during the 14 days preceding landslide occurrences. Key: in blue, red, and green: values from the Tramonti, Castellammare, and Tramonti-Chiunzi rain gauges, respectively. Numbers refer to id. in Table 1 (cf. first column).

portation facilities (Mele and Del Prete, 1999; Calcaterra and Santo, 2004; Di Crescenzo and Santo, 2005). In the second half of the twentieth century, several shallow landslides activated nearby Castellammare di Stabia: in Table 1, the major events recorded between Vico Equense and Gragnano are listed, with details on types of events, affected sites and references. The shallow landslides listed in Table 1 occurred between November and March, a period characterized by a medium to low suction range and included in the rainy season (October to April), according to Cascini et al. (2014). The same authors pointed out that, in this period, frontal rainfall typically occurs and may trigger widespread first-time shallow landslides, later propagating as debris flow or debris avalanches.

Rainfall responsible for landslide occurrences in the Sorrento Peninsula is shown in Fig. 7, in terms of cumulated antecedent rains, extracted from the records of the nearest gauges (Tramonti, Castellammare, and Tramonti-Chiunzi – cf. Fig. 6). The trends of antecedent rains look quite different, ranging from abrupt (cf. curves 5, 6, 7) to progressive increases (cf. 2, 4, 10). On the other hand, curve 0 does not highlight significant amounts of rainfall in the 14 days preceding landslide activation: therefore, the occurrence recorded on 14 April 1967 was excluded from the hydrological analysis. Quite moderate amounts of cases 6 and 7 (that occurred on 4 November 1980 and 14 November 1982, respectively) were instead recorded in short periods, thus resulting in high-intensity events that could be considered as the triggering factor of the observed landslides.

As a result, the dates of activation from no. 1 to no. 10 were selected for calibration, whilst no. 11 was employed for validation. As shallow landslides were being considered, the rainfall period employed for calibration spanned from 17 January 1963 to 10 December 1996; for validation, the rainfall series extended from 11 December 1996 to 10 February 1997 – i.e., to the validation date $+t_b$ (this latter as obtained from calibration).

4.2 The Uncino landslide – San Fili (northern Calabria)

San Fili (Fig. 8) is located on the western margin of the Crati *graben*, a tectonic depression along the active Calabrian–Sicilian rift zone (Monaco and Tortorici, 2000). In the area, vicarious, N–S trending normal faults mark the base of the coastal chain, at the transition between Palaeozoic metamorphic rocks, to the west, and Pliocene–Quaternary sediments, to the east (Amodio Morelli et al., 1976). Nearby San Fili, Palaeozoic migmatitic gneiss and biotitic schist, generally weathered, are mantled by a late Miocene sedimentary cover of reddish continental conglomerate, followed by marine sandstone and clays (CASMEZ, 1967). In particular, the village lies in the intermediate sector between two faults, marked by a NE–SW trending connection fault, delimiting Miocene sediments, to the north, from gneissic rocks, to the south.

In Calabria, the Tyrrhenian sector (including the study area) results are rainier than the Ionian sector (about 1200–2000 mm vs. 500 mm). Nevertheless, the most severe storms occur more frequently in the Ionian sector (Terranova, 2004). The average annual temperature is about 15 °C: the coldest months are January and February (on average, 5 °C), fol-

Table 2. Dates of activation of the Uncino landslide. Periods (instead of singular dates) were considered in case of uncertain timing of activation. Key = no.: identification number of the date (in bold, used for calibration); dates/periods derived from the literature; dates/periods employed for calibration or validation; references: sources of information on activation dates; rank: relative position and dates of the maxima of the mobility function during calibration. An asterisk marks the activation employed for validation. In italics, the activation date (no. 0) excluded due to hydrological constraints.

No.	Date	Reference	Period	Rank
1	16, 21 Jan 1960	Sorriso-Valvo et al. (1996)	16–21 Jan 1960	18 Jan 1960 (5)
2	Winter 1963	Sorriso-Valvo et al. (1994)	01 Nov 1962–14 Apr 1963	29 Mar 1963 (1)
3	15 Apr 1964 (h 22:00)	Sorriso-Valvo et al. (1994)	15 Apr 1964	14 Apr 1964 (3)
4	14 Dec 1966	Lanzafame and Mercuri (1975)	14 Dec 1966	16 Dec 1966 (2)
5	10–14, 21 Feb 1979	Sorriso-Valvo et al. (1994)	10–21 Feb 1979	15 Feb 1979 (4)
6	December 1980	Sorriso-Valvo et al. (1994)	01–31 Dec 1980	*
0	*23 Nov 1988*	*Sorriso-Valvo et al. (1996)*	–	–

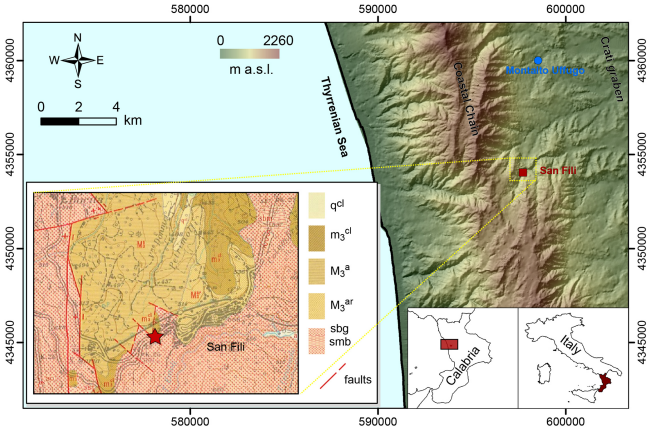

Figure 8. Location of the study area (red square: San Fili village; blue circle: Montalto Uffugo rain gauge). On bottom left, an extract from the geological map of Calabria (CASMEZ, 1967). Key: (sbg) gneiss and biotitic schist with garnet (Palaeozoic); (sbm) schist including abundant granite and pegmatite veins, forming migmatite zones (Palaeozoic); (M_3^{ar}) arenite and silt with calcarenite (Late Miocene); (M_3^{a}) marly clay with arenite and marls (Late Miocene); (m_3^{cl}) reddish conglomerate with arenite (Late Miocene); (q^{cl}) loose conglomerate of ancient fluvial terraces (Pleistocene). The site affected by the Uncino landslide is marked by a red star.

lowed by December (8 °C); the hottest months are July and August (24 °C), followed by June (22 °C).

As in most of the region, the climate at San Fili is Mediterranean (Csa, according to Köppen, 1948). Being located on the eastern side of a ridge, the area is subject to *Föhn* conditions with respect to perturbations coming from the Tyrrhenian Sea. It is characterized by heavy and frequent winter rainfall, caused by cold fronts mainly approaching from the northwest, and autumn rains, determined by cold air masses from the northeast. In spring, rains show lower intensities than in autumn, whilst strong convective storms are common at the end of summer. The average monthly rains recorded at the Montalto Uffugo gauge (the closest to San Fili) are listed in Table 3. From October to March (i.e., the wet semester), 77 % of the annual rainfall is totalized in about 77 rainy days; 36 % of the annual rainfall is recorded in 38 days during the three wettest months; finally, from June to August (i.e., the three driest months), 6 % of the annual rains fall in 11 days.

The Uncino landslide is located at the western margin of San Fili (Fig. 8). It is a medium-size rock slide (maximum width = 200 m, length > 650 m, estimated maximum vertical depth = 25 m), with a deep-seatedness factor (sensu Hutchinson, 1995) that may be classified as "intermediate". The slope movement involves a late Miocene conglomerate, arenite and marly clay overlaying Palaeozoic gneiss and biotitic schist. It repeatedly affected the village, damaging the railway and the local road network, besides some buildings: the most ancient known activation dates back to the beginning of the twentieth century (Sorriso-Valvo et al., 1996); from 1960 to 1990, seven dates of mobilization are known (as listed in Table 2). In such events, the railroad connecting Cosenza to Paola was damaged or even interrupted. By the way, on 28 April 1987, the railway was put out of service; hence, the relevance of the infrastructure decreased, together with media attention. Usually, such information is collected from archives not compiled by landslide experts, and is therefore affected by intrinsic uncertainty (e.g., concerning the dates of activity, and the partial or total activation of the phenomenon), with unavoidable problems of homogeneity of the data employed for model calibration.

The informative content of the Uncino case study is quite high, and allows for a more accurate calibration of the kernel with respect to the Sorrento Peninsula case: consequently, a smaller family of optimal solutions is expected. Nevertheless, the known activations still suffer from uncertainties related to dates and affected volumes.

Cumulated antecedent rains, corresponding to the Uncino landslide occurrences, are shown in Fig. 9. Rainfall data were extracted from the records of the Montalto Uffugo rain gauge (cf. Fig. 8). The trends of antecedent rains may be distin-

Table 3. Average monthly rainfall and number of rainy days at the Montalto Uffugo rain gauge (468 m a.s.l.).

	Sep	Oct	Nov	Dec	Jan	Feb	Mar	Apr	May	Jun	Jul	Aug	year
Rainfall (mm)	70.4	125.1	187.9	220.8	198.1	160.3	132.8	98.9	64.6	27.8	18.3	28.6	1333.6
Rainy days	6.9	10.6	12.8	14.3	14.3	12.5	12.6	10.7	8.26	4.7	2.62	3.84	114.0

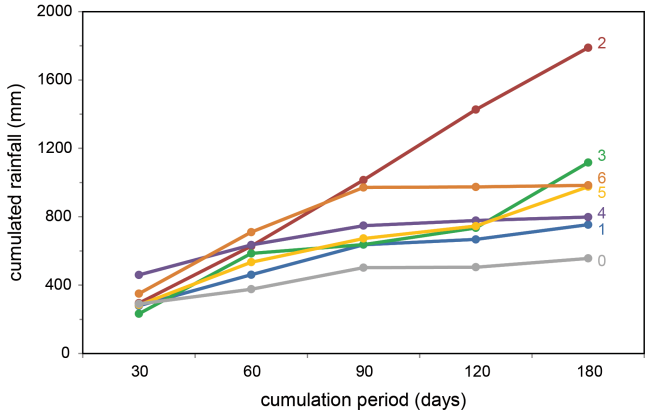

Figure 9. Cumulative daily rainfall (in mm) from 30 to 180 days before landslide occurrences (Montalto Uffugo gauge). Numbers refer to the identification number (no.) in Table 2 (cf. first column).

guished into 3 main patterns: the curve 2 shows a constant increase of rainfall in time, totalizing the greatest amounts from ca. 90 to 180 days. On the other hand, the case 0 shows the lowest values throughout the considered accumulation period. The curves 1, 3, 4, and 5 totalize intermediate values, with abrupt increases from 120 to 180 days for curves 3 and 5. Finally, the case 6 looks similar to case 2 between 30 and 90 days, but shows no more increases in the remaining period (analogously to 1 and 4).

As curve 0 does not highlight significant amounts of rainfall in the 30–180 days preceding the landslide activation, the occurrence recorded on 23 November 1988 was excluded from the hydrological analysis. Of the remaining curves, case 1 generally shows the lowest amounts, from ca. 40 to 180 days. Consequently, the dates of activation from no. 1 to no. 5 were selected for calibration, whilst no. 6 was employed for validation. Since a medium-size landslide was being considered, the rainfall period employed for calibration spans from 01 September 1959 to 31 August 1980; for validation, it ranges from 01 September 1980 to 31 March 1981 – i.e., including the validation date by $\pm t_b$ (this latter as obtained from calibration).

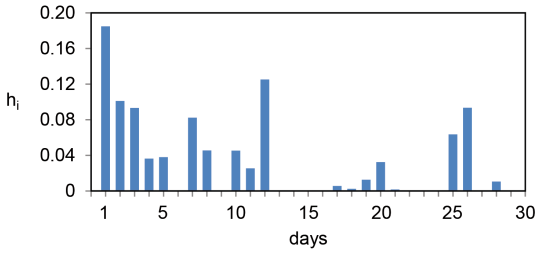

Figure 10. Sorrento Peninsula case study. Average kernel obtained from the 100 best filter functions.

5 Results

GA*SAKe* was applied to shallow-landslide occurrences in the Sorrento Peninsula and to a medium-size slope movement at San Fili, by considering the dates of activation and the daily rainfall series mentioned in Sects. 4.1 and 4.2, and adopting the values of parameters listed in Table 4.

Among the kernels obtained from calibration, several provided similar fitness values. Thus, "average kernels" were computed for the considered case studies, by averaging the 100 best kernels.

5.1 Application to shallow landslides in the Sorrento Peninsula

In Table 5, the statistics related to the 100 best filter functions obtained from calibration (optimal kernels) are summarized. From such values, a low variability of Φ, t_b and μ_0 can be appreciated; instead, Δz_{cr} shows a greater range of values. The average kernel is shown in Fig. 10: it is characterized by fitness $= 0.806$, $\Delta z_{cr} = 0.00282$, and $t_b = 28$ days. From such a kernel, antecedent rainfall mostly affecting landslide instability ranges from 1 to 12 days, and subordinately from 25 to 26 days (negligible weights refer to rains that occurred in the remaining period).

The mobility function related to the average kernel is shown in Fig. 11. In this case, 4 out of 10 dates of landslide activation are well captured by the model (being ranked at the first 7 positions of the mobility function maxima); the remaining 6 dates do also correspond to relative maxima of the function, but are ranked from the 43rd to the 151st position. When considering the remaining relative maxima, several false positives can be recognized, mainly up to 1979.

During calibration, the best fitness ($\Phi = 0.807$) was first reached after 1749 iterations (at 6th individual), with

Table 4. Values of the parameters of GASAKe adopted in the calibration procedure (benchmark experiment).

Symbol	Parameter	Value
N	Individuals of each GA population	20
t_b	Base time (Uncino landslide)	30/180 days
	Base time (shallow landslides in the Sorrento Peninsula)	2/30 days
p_{mh1}	Percentages of the maximum height of the kernel,	50 %,
p_{mh2}	used to define the range in which dh is randomly obtained	150 %
p_c	Probability of crossover	75 %
p_m	Probability of mutation	25 %
p_{me}	Number of mutated elements of the kernel, expressed as a percentage of t_b	25 %
p_{mtb}	factor defining the range in which dt_b is selected	0.2/5
Λ	Number of GA iterations (Uncino landslide case study)	5000
	Number of GA iterations (Sorrento Peninsula case study)	3000
n_e	Number of "elitist" individuals	8

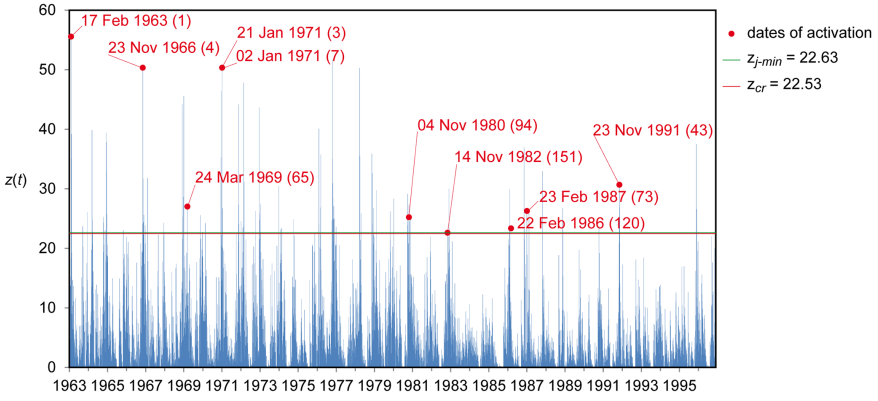

Figure 11. Sorrento Peninsula case study. Mobility function, $z(t)$, of the average kernel. The red line ($z_{cr} = 22.53$) shows the maximum value of the mobility function (critical condition) that is unrelated to known landslide activations. The green line ($z_{j-min} = 22.63$) – almost overlapping with the red line in this case – shows the minimum value of the mobility function related to known landslide activations. When the mobility function exceeds the threshold marked by the red line, landslide activation may occur. The red dots represent the maxima of the mobility function corresponding to the dates of landslide activation considered for calibration.

Table 5. Sorrento Peninsula case study. Statistics for the 100 best kernels.

	Φ	Δz_{cr}	t_b	μ_0
Min	0.806	3.82×10^{-5}	26.0	9.460
Average	0.806	0.00418	30.4	9.567
Max	0.807	0.00801	31.0	10.448
Median	0.806	0.00499	31.0	9.567
Mode	0.806	0.00499	31.0	9.567
SD	7.65×10^{-5}	0.00183	0.862	0.146

$\Delta z_{cr} = 0.00441$ and $t_b = 26$ days. The kernel corresponding to such individual looks similar to the best one in terms of $t_b, \Delta z_{cr}$, and μ_0 (Fig. 12). The pattern of the best kernel is only slightly dissimilar from the average one: significant weights can, in fact, be appreciated up to 14 days, and then between 20–22 and 25–26 days.

By applying the average kernel, a validation was performed against the remaining date of activation (cf. Table 1, no. 11; multiple events occurred on 10 January 1997). The validation that resulted was fully satisfied, as shown in Fig. 13: the value of the mobility function for event no. 11 is well above the z_{cr} threshold (49.01 vs. 18.05), and is ranked as the second highest value among the function maxima (Fig. 13a). The same peak can also be appreciated as the maximum of the period $\pm t_b$ (Fig. 13b). Accordingly, when adopting the average kernel, event no. 11 of landslide activation could properly be predicted by the model.

5.2 Application to the Uncino landslide

In Table 6, the statistics related to the family of optimal kernels are summarized. From such values, a low variability of t_b and Δz_{cr} can be appreciated. The average kernel (Fig. 14) is characterized by fitness = 1, $\Delta z_{cr} = 0.0644$, and $t_b = 66$ days. Based on such a kernel, antecedent rains from

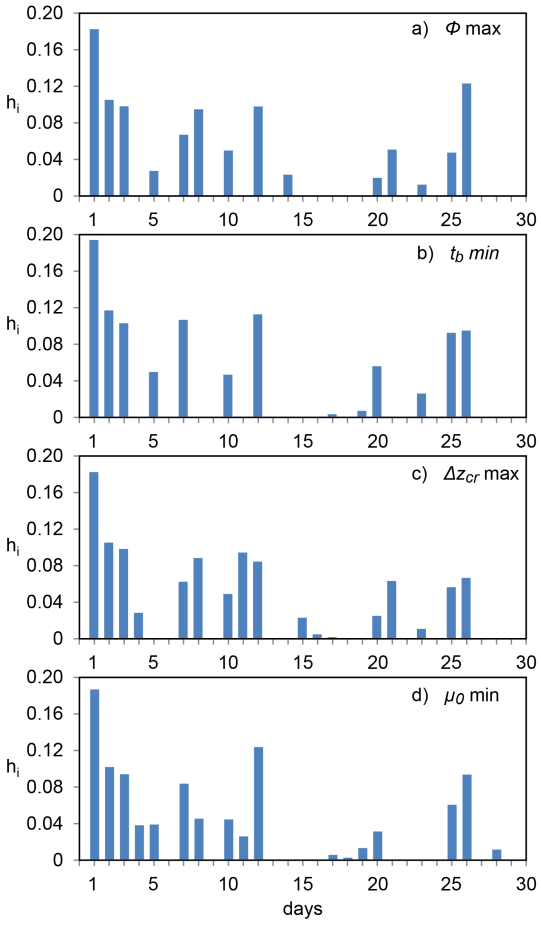

Figure 12. Sorrento Peninsula case study. Kernels providing **(a)** the best fitness ($\Phi_{max} = 0.807$), **(b)** the minimum base time t_b min (26 days), **(c)** the Δz_{cr} max (0.00801), and **(d)** the minimum first-order momentum, μ_0 min (9.460).

Table 6. Uncino landslide case study. Statistics for the 100 best kernels.

	Δz_{cr}	t_b
Min	0.0524	57.0
Average	0.0581	69.5
Max	0.0692	82.0
Median	0.0581	69.0
Mode	0.0558	69.0
SD	0.00373	3.12

1 to 17 days, and from 27 to 45 days, mainly affect landslide instability. Relatively smaller weights pertain to the rains that occurred more than 53 days before the triggering; for periods older than 66 days, the weights are negligible.

In Fig. 15, the mobility function related to the average kernel highlights that all the 5 dates of activation are well captured by the model (they are ranked at the first 5 positions among the function maxima). When considering the remaining relative maxima of the function, only 4 of them evidence quasi-critical situations (between 1965 and 1966, and subordinately in 1970 and 1977).

Table 7. Uncino landslide case study. Results of progressive calibration. Key: L, t_b, z_{j-min}, z_{cr}, Δz_{cr}): model parameters concerning calibration (for explanation, cf. text); Φ_v) fitness obtained by validating the "average kernel", obtained in calibration, against the 6 dates of activation. In italics, results obtained when calibrating the model by using all the six available dates (no validation performed).

L	t_b	z_{j-min}	z_{cr}	Δz_{cr}	Φ_v
2	30	13.93	13.89	0.0029	0.59
3	54	11.05	11.04	0.0009	0.78
4	55	10.21	10.20	0.0010	0.87
5	80	16.44	16.34	0.0061	0.95
6	*80*	*18.63*	*17.43*	0.0644	*1.00*

During calibration, the best fitness ($\Phi = 1$) was first reached after 684 iterations (at 13th individual) with $\Delta z_{cr} = 0.0595$. The best kernel (Fig. 16) was obtained at iteration 993, at 8th individual, with $\Delta z_{cr} = 0.0631$. Its pattern results very similar to the average one, with a t_b of 66 days.

By applying the average kernel, a validation was performed against the last known date of activation (cf. Table 2, no. 6, which occurred in December 1980). The validation that resulted was fully satisfied, as shown in Fig. 17: the value of the mobility function for event no. 6, in fact, is well above the z_{cr} threshold (17.49 vs. 16.87), and is ranked as the sixth highest value among the function maxima (Fig. 17a). The same peak can be appreciated as the maximum of the period $\pm t_b$ (Fig. 17b). Accordingly, when adopting the average kernel, event no. 6 could properly be predicted by the model.

6 Self-adaptive procedure and sensitivity analyses

The capability of the model to react and self-adapt to input changes, such as new dates of landslide activation, was evaluated by a progressive, self-adaptive procedure of calibration and validation, using the information available for the Uncino case study. To simulate the adoption of GASAKe in a landslide warning system, the model was iteratively calibrated by the first 2, 3, 4, and 5 dates of activation (L), and validated against the remaining 4, 3, 2, 1 dates, respectively. In each experiment, the GA parameters listed in Table 4 were adopted. Finally, the model was merely calibrated by considering all the 6 dates of activation. The results of the self-adaptive procedure are listed in Table 7. The related kernels are shown in Fig. 18. As a result, a progressive increase in fitness and predictive ability (Δz_{cr}), together with the base time (ranging from 30 to 80 days), can be appreciated when employing a greater number of dates of activation.

Furthermore, aiming at evaluating the sensitivity of the model with respect to the GA parameters, a series of anal-

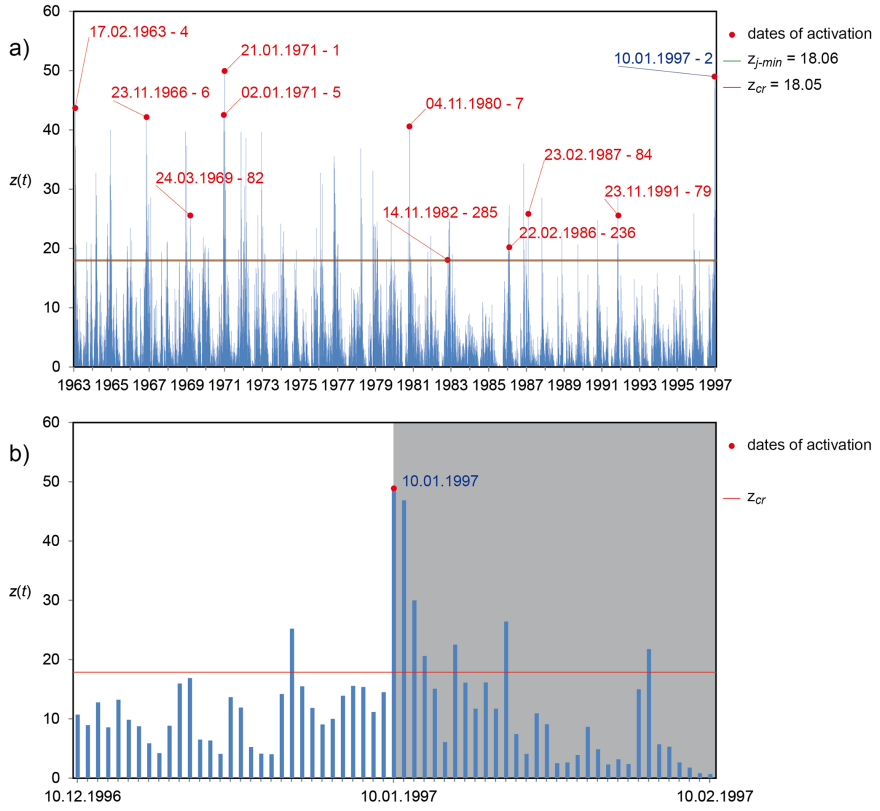

Figure 13. Sorrento Peninsula case study. **(a)** Validation of the average kernel against the no. 11 event. **(b)** Particular of **(a)**, limited to the period $\pm t_b$, including the date of validation. Key as in Fig. 11. The blue label indicates the date of validation. Grey background marks the period after the event that may be employed for re-calibration.

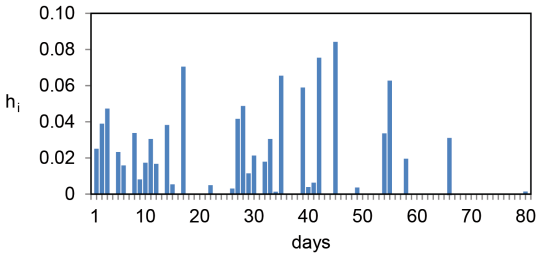

Figure 14. Uncino landslide case study. Average kernel obtained from the 100 best filter functions.

yses was performed by considering again the Uncino case study. The experiments carried out are listed in Table 8. Each simulation stopped after 1500 iterations: GA parameters were initialized by considering the "benchmark experiment" (cf. values in Table 4), except for the parameter that was in turn varied, as indicated in Table 8. The obtained maximum fitness (Φ_{max}), safety margin (Δz_{cr}), number (n_i) of iterations needed to first reach Φ_{max}, and base time (t_b) of the average kernel are shown in Fig. 19. If experiments with $\Phi_{max} = 1$ are only taken into account, the minimum and maximum numbers of GA iterations needed to reach

Table 8. Uncino landslide case study. Values of the parameters adopted in the sensitivity analyses. In bold, the experiments with $\Phi_{max} = 1$. In italics, the worst experiment. Underlined, the best one.

Symbol	Values				
n_e	**6**	**7**	**8***	**9**	**10**
p_c	60 %	67.5 %	**75 %***	*82.5 %*	90 %
p_m	20 %	**22.5 %**	**25 %***	**27.5 %**	30 %
p_{mh1}	60 %	**55 %**	**50 %***	45 %	40 %
p_{mh2}	140 %	**145 %**	**150 %***	155 %	160 %
p_{me}	20 %	22.5 %	**25 %***	27.5 %	**30 %**
p_{mtb}	**0.25/4**	0.22/4.5	**0.2/5***	**0.18/5.5**	0.17/6
N, n_e		**25, 8**	**20, 8***	**15, 8**	
N, n_e		**25, 12**	**25, 10**	**25, 8**	

* Reference values (i.e., those of the benchmark experiment – cf. Table 4).

Φ_{max} (Λ_{min}, Λ_{max}), the minimum and maximum base times of the average kernel (t_{b_min}, t_{b_max}), and the minimum and maximum safety margins of the average kernel (Δz_{cr_min}, Δz_{cr_max}), are listed in Tables 9, 10 and 11, respectively.

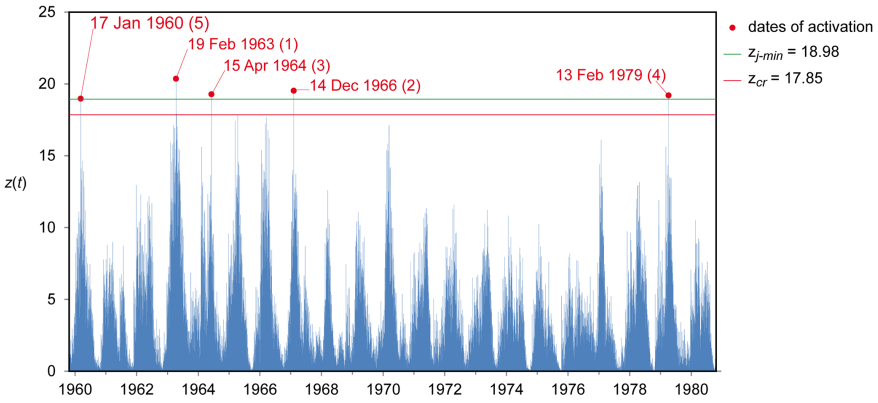

Figure 15. Uncino landslide case study. Mobility function, $z(t)$, of the average kernel. The red line ($z_{\mathrm{cr}} = 17.85$) shows the maximum value of the mobility function (critical condition) that is unrelated to known activations. The green line ($z_{j-\mathrm{min}} = 18.98$) shows the minimum value of the mobility function related to known activations. When the mobility function exceeds the threshold marked by the red line, landslide activation may occur. The red dots represent the maxima of the mobility function corresponding to dates of landslide activation considered for calibration.

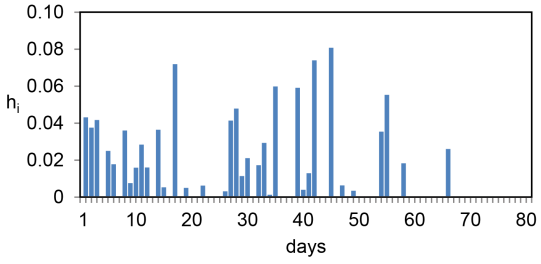

Figure 16. Uncino landslide case study. Kernel providing the best fitness.

7 Discussion and conclusions

In the present paper, the GA*SAKe* model is presented with examples of application to shallow landslides in the Sorrento Peninsula (Campania), and to the medium-size Uncino landslide at San Fili (Calabria). Furthermore, the capability of the model to simulate the occurrence of known landslide activations was evaluated by a progressive, self-adaptive procedure of calibration and validation against the Uncino case study. Finally, the sensitivity of the model with respect to the GA parameters was analyzed by a series of experiments, performed again by considering the latter landslide.

Regarding the Sorrento Peninsula case study, the maximum fitness obtained during calibration is smaller than unity. For the 100 best kernels, Φ_{max}, Δz_{cr} and t_{b} vary in a small range (ca. 0.1, 4.8, and 13 %, respectively). Furthermore, as mentioned above, for specific types of application (e.g., civil protection), the observed small values of Δz_{cr} would imply short warning times. Consequently, a suitable kernel should be rather selected by privileging the shortest t_{b} or the smallest μ_0. From Fig. 12, it can be noticed that the greatest weights for the first 12–15 days are obtained by selecting the kernel characterized by the smallest μ_0, thus allowing for the most timely advice if used within an early-warning system. In the average kernel, the greatest weight can be attributable to the first 12 days, with a maximum base time of about 4 weeks, reflecting the general shape of the curves in Fig. 7, and in good agreement with the shallow type of slope instability considered. Furthermore, the validation of the average kernel is satisfactory, as the validation date (no. 11 in Table 1) corresponds to the second highest peak of the mobility function. In addition, no missing alarms and only four false alarms in about 5 years are to be found (i.e., in the period from the last date used for calibration to the one for validation). The peaks

Table 9. Minimum (Λ_{i_min}) and maximum (Λ_{i_max}) numbers of GA iterations needed to reach Φ_{max} (only experiments with $\Phi_{\mathrm{max}} = 1$ are considered). In the first column, the letters refer to Fig. 19. In bold, the best and worst experiments. An asterisk marks the experiment *e*, in which Φ_{max} was reached only for $p_{\mathrm{c}} = 75$. In italics, the combinations of parameters of the benchmark experiment (cf. Table 4).

§	N	Parameter	Λ_{i_min}	Λ_{i_max}
a	*20*	$n_{\mathrm{e}} = 8$		*684*
a	20	$n_{\mathrm{e}} = 10$	**279**	
c	25	$n_{\mathrm{e}} = 8$	469	
c	25	$n_{\mathrm{e}} = 12$		**1477**
e	*20*	$p_{\mathrm{c}} = 75$	*684**	
g	*20*	$p_{\mathrm{m}} = 25$	*684*	
g	20	$p_{\mathrm{m}} = 27.5$		1086
i	*20*	$p_{\mathrm{mh1}} = 50$	*684*	
i	20	$p_{\mathrm{mh1}} = 55$		836
k	*20*	$p_{\mathrm{me}} = 25$	*684*	
k	20	$p_{\mathrm{me}} = 30$		996
m	*20*	$p_{\mathrm{mtb}} = 5$	*684*	
m	20	$p_{\mathrm{mtb}} = 5.5$		1052
o	15	$n_{\mathrm{e}} = 8$	405	

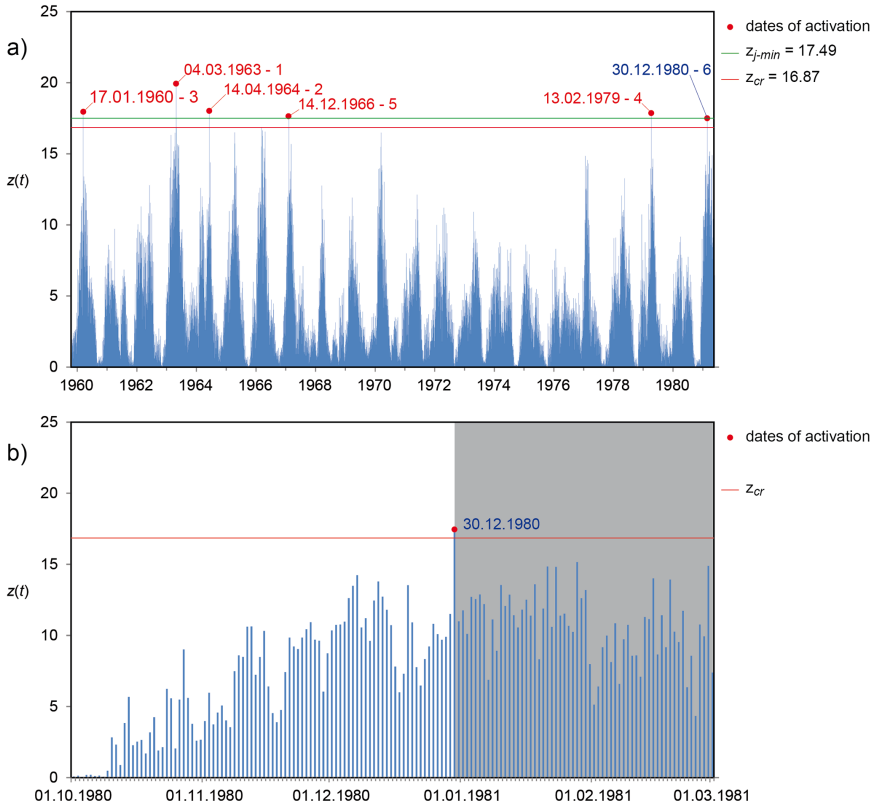

Figure 17. Uncino landslide case study. **(a)** Validation of the average kernel against the no. 6 event. **(b)** Particular of **(a)**, limited to the period $\pm t_b$ including the date of validation. Key as in Fig. 15. The blue label indicates the date of validation. Grey background marks the period after the event that may be employed for re-calibration.

Table 10. Minimum (t_{b_min}) and maximum (t_{b_max}) base times of the average kernel (only experiments with $\Phi_{max} = 1$ are considered). In the first column, the letters refer to Fig. 19. In bold, the best and worst experiments. An asterisk marks the experiment *e*, in which Φ_{max} was reached only for $p_c = 75$. In italics, the combinations of parameters of the benchmark experiment (cf. Table 4).

§	*N*	Parameter	t_{b_min}	t_{b_max}
a	*20*	$n_e = 8$	*66.59*	
a	20	$n_e = 10$		144.85
c	25	$n_e = 8$		132.00
c	25	$n_e = 12$	56.17	
e	*20*	$p_c = 75$	*66.59**	
g	*20*	$p_m = 25$	*66.59*	
g	20	$p_m = 27.5$		139.20
i	*20*	$p_{mh1} = 50$		*66.59*
i	20	$p_{mh1} = 55$	**44.00**	
k	*20*	$p_{me} = 25$	*66.59*	
k	20	$p_{me} = 30$		**146.93**
m	*20*	$p_{mtb} = 5$	*66.59*	
m	20	$p_{mtb} = 4$		136.06
o	15	$n_e = 8$		145.79

Table 11. Minimum (Δz_{cr_min}) and maximum (Δz_{cr_max}) safety margins of the average kernel (only experiments with $\Phi_{max} = 1$ are considered). In the first column, the letters refer to Fig. 19. In bold, the best and worst experiments. An asterisk marks the experiment *e*, in which Φ_{max} was reached only for $p_c = 75$. In italics, the combinations of parameters of the benchmark experiment (cf. Table 4).

§	*N*	Parameter	Δz_{cr_min}	Δz_{cr_max}
a	20	$n_e = 7$		0.007
a	20	$n_e = 9$	0.002	
c	25	$n_e = 8$		0.014
c	25	$n_e = 12$	0.002	
e	*20*	$p_c = 75$	*0.005**	
g	20	$p_m = 22.5$		0.006
g	20	$p_m = 27.5$	**0.001**	
i	*20*	$p_{mh1} = 50$		*0.005*
i	20	$p_{mh1} = 55$	0.004	
k	*20*	$p_{me} = 25$	*0.005*	
k	20	$p_{me} = 30$		0.006
m	*20*	$p_{mtb} = 5$	*0.005*	
m	20	$p_{mtb} = 4$		0.009
o	15	$n_e = 8$		**0.055**
o	*20*	$n_e = 8$	*0.005*	

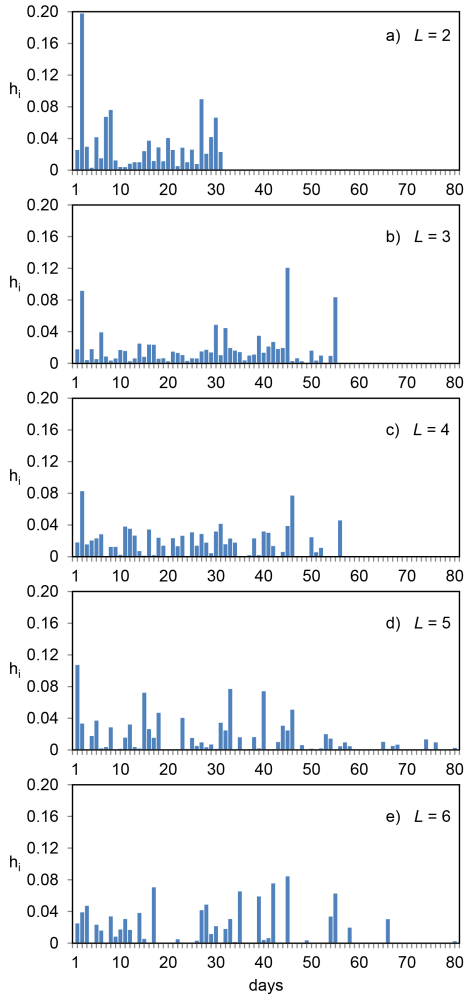

Figure 18. Uncino landslide case study. Average kernels obtained in calibration against the 2, 3, 4, 5, and 6 dates of activation.

of the mobility function corresponding to the activation dates can roughly be grouped into two sets, characterized by distinct values: a first set, with $z(t) > 40$, generally includes the most ancient plus the validation dates (no. 1, no. 2, no. 4, no. 5, no. 6, and no. 11); a second set, with $18 < z(t) < 25$, includes nos. 3, 7, 8, 9, and 10. False alarms result more frequently and higher in the first period (from 1963 to 1980), presumably due to a lack of information on landslide activations.

Regarding the Uncino case study, the maximum fitness in calibration reaches unity. With respect to the Sorrento Peninsula case study, Δz_{cr} and t_b of the 100 best kernels vary in a greater range (ca. 25 and 30.5 %, respectively), with Δz_{cr} 1 order of magnitude greater. In this case, the kernel would in fact allow for a safety margin of ca. 5 %. In the average kernel, three main periods can be recognized with heavier weights, attributable to (i) the first 17 days, (ii) 27–45 days, and (iii) 54–58 days. The base time ranges from about 8 to 12 weeks, in good agreement with the medium-size type of the considered slope instability. Furthermore, the validation of the average kernel was performed successfully: in fact, the validation date (no. 6 in Table 2) corresponds to the third highest peak of the mobility function; even in this case, neither missing alarms nor false alarms in about 2 years (from the last date calibration date to the validation one) are to be found. The peaks of the mobility function corresponding to the activation dates are characterized by $z(t) > 18$.

In the self-adaptive procedure applied to the Uncino case study, values for $L = 6$ merely refer to calibration, whilst the ones for $2 \leq L \leq 5$ concern validation. With regard to Table 7 and Fig. 20, it can be noticed that

- for $2 \leq L \leq 5$, t_b increases 2.7 times with L, and then remains constant for $L \geq 5$;
- from $L = 2$ to $L = 4$, $z_{j-\min}$ and z_{cr} slightly decrease, and then abruptly increase for $L \geq 5$;
- for $L \geq 4$, Δz_{cr} monotonically increases 72 times with L (being almost constant in the 2–4 transition);
- Φ_v monotonically increases 1.7 times with L.

As a whole, a satisfying performance is obtained starting from three dates (i.e., correct predictions in more than three out of four times). For $L = 5$, only one false alarm is observed. Finally, the calibration performed by considering all six dates of activation provided fully satisfying results. Accordingly, the results of the progressive procedure underlined how GA*SAKe* can easily self-adapt to external changes by optimizing its performances, providing increasing fitness values.

The average kernels obtained by considering two to six dates of landslide activation show increasing base times, with significant weights for the most ancient rains of the temporal range (Fig. 18). Such a result is in good accordance with the extent of the slope movement and, therefore, with the expected prolonged travel times of the groundwater affecting landslide activation.

In the sensitivity analyses, again performed by considering the Uncino landslide, $\Phi_{max} = 1$ was obtained in 60 % of the experiments (cf. Table 8). The results (cf. Fig. 19 and Tables 9, 10, and 11) permit one to select the set of parameters that allow for faster GA performances. More in detail,

- a ratio between the number of elitist individuals and the whole population of $n_e/N = 10/20$ or 8/15 allows for the fastest GA performances ($\Lambda_{i\_\min} \sim 41$ % of the reference value); nevertheless, for increasing both n_e and N, this effect seems to vanish (e.g., $n_e/N = 12/25$);
- with respect to the benchmark experiment, the explored changes in p_c, p_m, p_{mh1}, p_{me}, and p_{mtb} do not substantially affect the GA performances with respect to $\Lambda_{i\_\min}$;

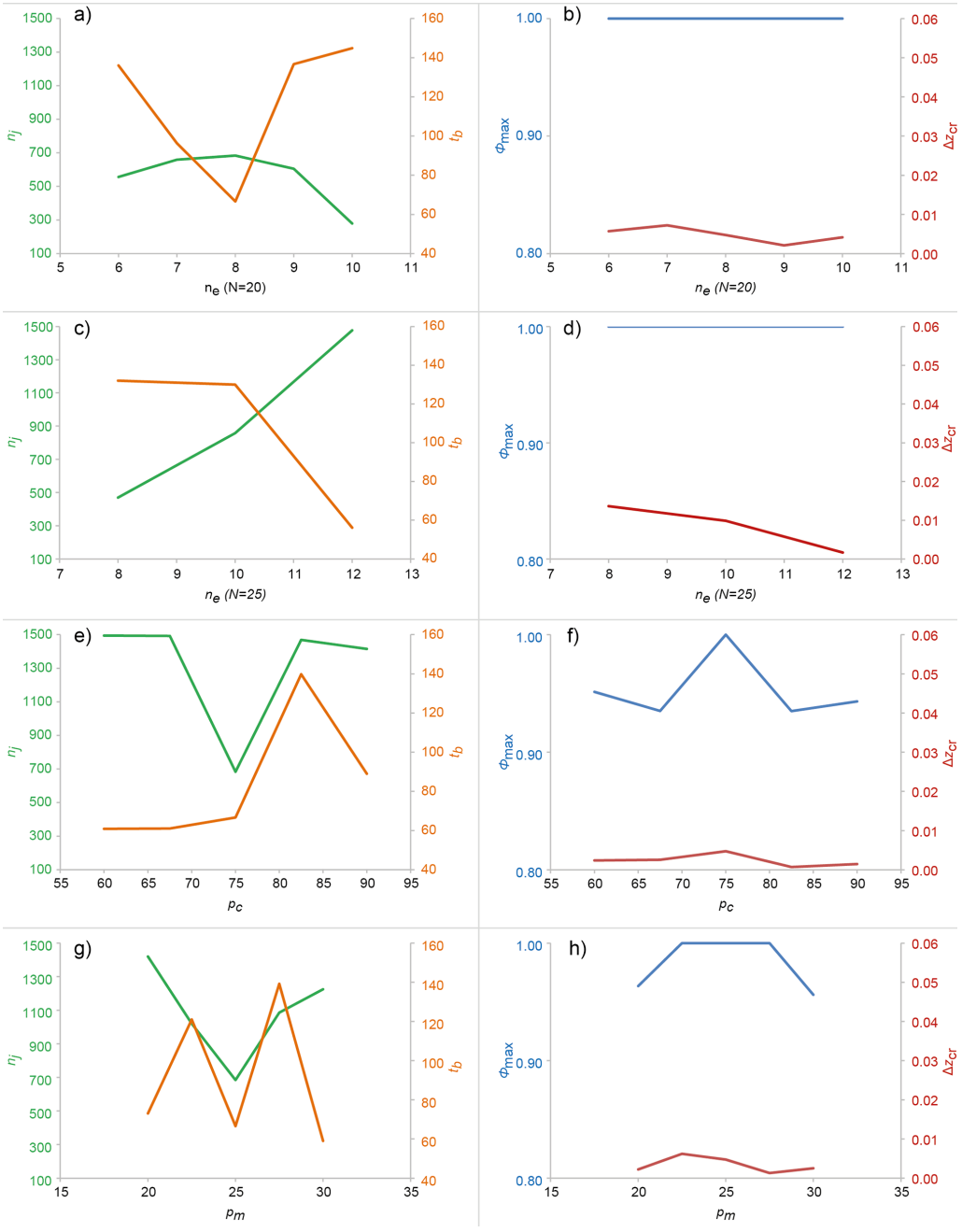

Figure 19.

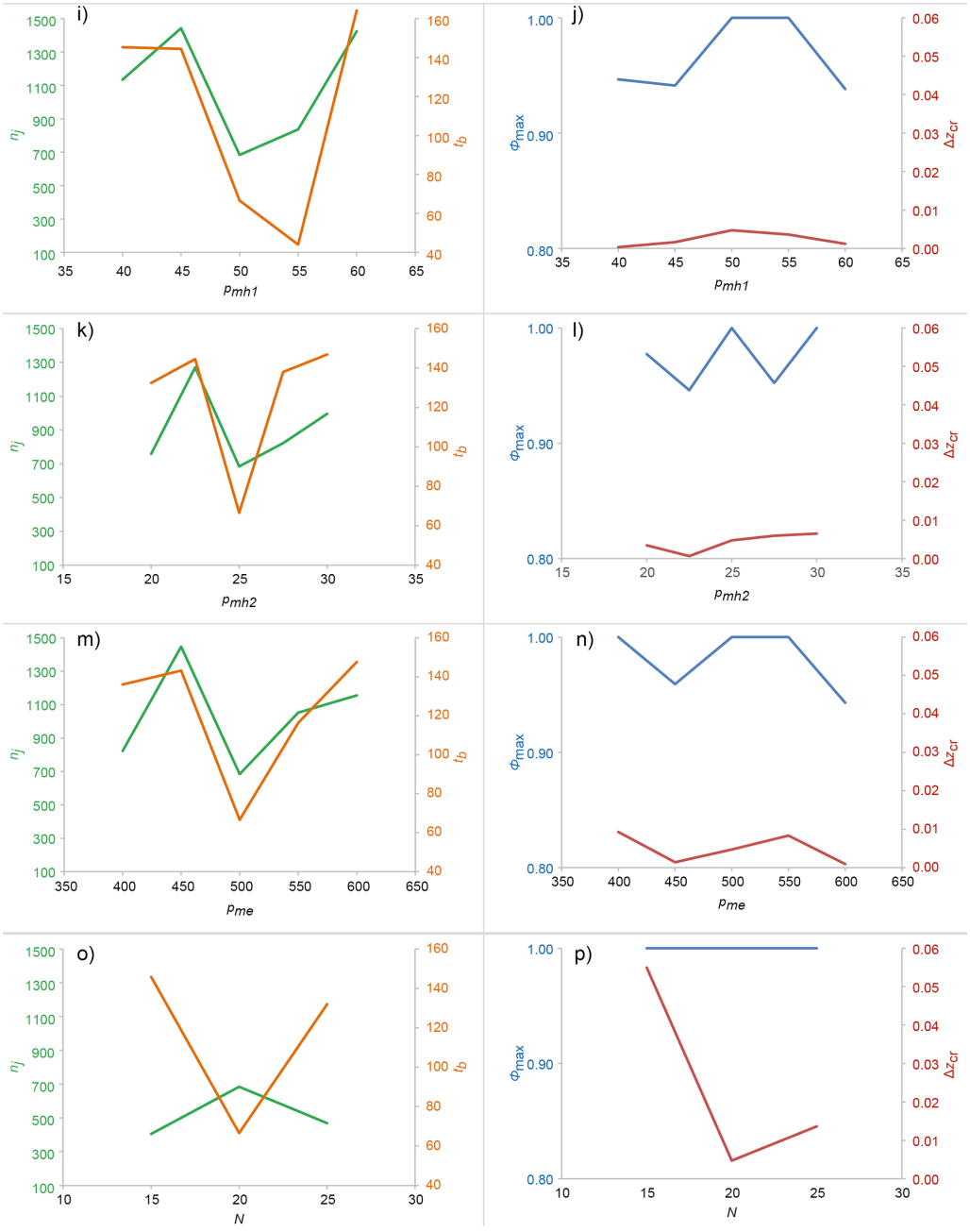

Figure 19. Maximum fitness (Φ_{max}), safety margin (Δz_{cr}), number (n_i) of iterations needed to first reach Φ_{max}, and base time (t_b) of the average kernel, based on GA parameters listed in Table 8.

– with respect to the benchmark experiment, the explored changes of parameters determine the variation of t_b from 66 to 219 %;

– in case of civil protection applications, the combination of parameters with $p_{mh1} = 55$ allows for activating early-warning procedures with the greatest advance; and

– concerning Δz_{cr_max}, the best result (increase by 10 times) is obtained when reducing N to 15.

The calibration experiments discussed in this paper were performed on a standard PC platform (3 GHz CPU, 4 GB RAM, SQL stand-alone system and application process). For the study cases of the Sorrento Peninsula and the Uncino landslide, 2.5 and 1.1 GA iterations were, respectively, performed per minute, reaching Φ_{max} in 11 h 40 m and 10 h 20 m. Depending on the availability of high-performance

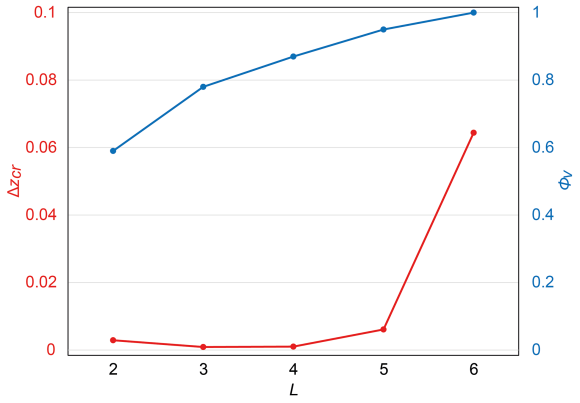

Figure 20. Uncino landslide case study. Results of progressive calibration. Variation of Δz_{cr} and Φ_v for L increasing from 2 to 6.

computing clusters, the mentioned durations may strongly be reduced, thus allowing for prompt civil protection applications, e.g., based on short-term weather forecasts. By the way, the time needed to calibrate the model can profitably be shortened by properly initializing the kernel, based on expected characteristics of the phenomena under consideration (e.g., the range of t_b strongly depends on landslide size).

In this study, a two-step efficiency criterion was employed: the relative position of the peaks of the mobility function with respect to the dates of landslide activation was first considered, and the fitness computed. Based on the value of Δz_{cr}, the obtained solutions were further ranked. Average, synthetic filter functions could then be computed by selecting the 100 best kernels for successive validation purposes. Alternative metrics (cf. among others, Krause et al., 2005) for the fitness function are being tested. However, due to uncertainties concerning input data (i.e., rainfall and dates of landslide activation), the adoption of sophisticated techniques does not sound very promising. In addition, problems of over-fitting may depend on both data uncertainties and the number of parameters. Commonly, kernels characterized by a complex pattern (and then by many parameters) are needed for simulating groundwater dynamics (Pinault et al., 2001). Nevertheless, more complex kernels do not necessarily imply higher predictive uncertainties (Fienen et al., 2010; Long, 2015). Still, the adopted discrete approach allows one to focus only on the timing of the peaks of the mobility function, thus somewhat relieving the computational effort. Due to the cited uncertainties in input data, a "temporal window" was in fact employed to help in matching dates of activation with the peaks of the mobility function. Further attempts at defining the fitness function by different metrics, and the analysis of its effects on calibration and validation, are being considered against another case study (San Benedetto Ullano, in Calabria, southern Italy), whose mobility phases have been recently monitored by the same authors (Iovine et al., 2010; Capparelli et al., 2012).

As mentioned above, model calibration may be hampered by either quality or completeness of input data. Commonly, missing dates of activation (mainly in remote periods or in isolated areas) and unsuitability of the rain gauge network (e.g., due to excessive distance of gauges from the landslides) negatively affect model results. Depending on the availability of new dates of activation, stemming from further mobilizations or improvement of historical investigations, the predictive capability of the model can be increased through additional calibrations, hence providing new families of optimal solutions, constituted by fewer, highly significant kernels.

The above considerations suggest an indirect link between the model – despite being empirical in type – and the physical characteristics of the slope movements (e.g., dimensions, permeability, initial water content of the slope, length of subsurface water paths). In general, to select the kernel to be applied, it is rather preferable to consider a set of optimal kernels or the average one, instead of a single solution.

Further efforts are in progress to improve the model and its chances of practical application, mainly concerning the implementation of different GA techniques of optimization (in addition to the elitist one, employed here), the parallelization of the model, and the adoption of a genetic programming approach. Finally, through the analytical study of the optimal kernels, a mathematical formulation of discrete filter functions is presently being attempted, aiming at synthesizing optimal and average kernels for an easier comparison with the results of other models available in the literature.

Code availability

The release by GA*SAKe* of the *Self Adaptive Kernel* model, discussed in this paper, has been developed by scientists working at CNR-IRPI under Microsoft Windows, Visual Studio, and SQL Server integrated development environment. It can be requested by the public to the corresponding author of the paper, together with examples of input data and technical support (a user manual is not available yet, but it should be released soon). The model is presently undergoing further refinements and developments, mainly concerning types of GA-selection techniques, the post-processing of the results in terms of continuous analytical functions, and the implementation of a library of case studies. The authors are willing to cooperate with external users to further improve the model through applications to case studies from different geo-environmental contexts.

Acknowledgements. For the rainfall series of the Calabrian rain gauges, we are grateful to Regione Calabria, R. Niccoli, Direttore del Centro Funzionale Multirischi dell'ARPACal.

For the rainfall series of the Campanian rain gauges, we are grateful to Regione Campania, G. Schiavone, Dirigente del Settore "Programmazione Interventi di Protezione Civile sul Territorio", and M. Biafore, Dirigente del Servizio 04, Responsabile CFD "Centro

funzionale per la previsione meteorologica e il monitoraggio meteo-idro-pluviometrico e delle frane".

Finally, we thank the Editors and two anonymous Referees for their constructive comments and insights that allowed us to considerably improve the manuscript.

Edited by: J. Neal

References

Aleotti, P.: A warning system for rainfall-induced shallow failures, Eng. Geol., 73, 247–265, 2004.

Alfieri, L., Salamon, P., Pappenberger, F., Wetterhall, F., and Thielen, J.: Operational early warning systems for water-related hazards in Europe, Environ. Sci. Policy, 21, 35–49, 2012.

Amodio-Morelli, L., Bonardi, G., Colonna, V., Dietrich, D., Giunta, G., Ippolito, F., Liguori, V., Lorenzoni, S., Paglionico, A., Perrone, V., Piccarreta, G., Russo, M., Scandone, P., Zanettin Lorenzoni, E., and Zuppetta, A.: L'arco calabro-peloritano nell'orogene appenninico-maghrebide, Mem. Soc. Geol. Ital., 17, 1–60, 1976 (in Italian).

AMRA: Overview of intense rainfall on volcanic soils–regional and local scale, in: SafeLand – Living with landslide risk in Europe: Assessment, effects of global change, and risk management strategies, edited by: Crosta, G. B., Agliardi, F., Frattini, P., and Sosio, R., 101–122, 2012.

Berti, M., Martina, M. L. V., Franceschini, S., Pignone, S., Simoni, A., and Pizziolo, M.: Probabilistic rainfall thresholds for landslide occurrence using a Bayesian approach, J. Geophys. Res., 117, F04006, doi:10.1029/2012JF002367, 2012.

Brand, E. W., Premchitt, J., and Phillipson, H. B.: Relationship between rainfall and landslides, in: Proceedings of the 4th International Symposium on Landslides, Toronto, vol. 1, BiTech Publishers, Vancouver, Canada, 377–384, 1984.

Brunetti, M. T., Peruccacci, S., Rossi, M., Luciani, S., Valigi, D., and Guzzetti, F.: Rainfall thresholds for the possible occurrence of landslides in Italy, Nat. Hazards Earth Syst. Sci., 10, 447–458, doi:10.5194/nhess-10-447-2010, 2010.

Brunsden, D.: Mudslides, in: Slope Instability, edited by: Brunsden, D. and Prior, D. B., John Wiley & Sons, London, 363–418, 1984.

Caine, N.: The rainfall intensity-duration control of shallow landslides and debris flows, Geograf. Ann., 62A, 23–27, 1980.

Calcaterra, D. and Santo, A.: The January 10, 1997 Pozzano landslide, Sorrento Peninsula, Italy, Eng. Geol., 75, 181–200, 2004.

Campbell, R. H.: Debris flow originating from soil slip during rainstorm in southern California, Q. J. Eng. Geol., 7, 377–384, 1975.

Cannon, S. H. and Ellen, S. D.: Rainfall conditions for abundant debris avalanches, San Francisco Bay region, California, California Geology, 38, 267–272, 1985.

Capparelli, G. and Versace, P.: FLaIR and SUSHI: two mathematical models for early warning of landslides induced by rainfall, Landslides, 8, 67–79, 2011.

Capparelli, G., Iaquinta, P., Iovine, G., Terranova, O. G., and Versace P.: Modelling the rainfall-induced mobilization of a large slope movement in northern Calabria, Nat. Hazards, 61, 247–256, 2012.

Carter, J.: The notion of Threshold: an investigation into conceptual accompaniment in Aristotle and Hegel, Conserveries mémorielles, 7, available at: http://cm.revues.org/431 (last access: 10 December 2014), 2010.

Cascini, L. and Versace, P.: Eventi pluviometrici e movimenti franosi, in: Atti del XVI Convegno Nazionale di Geotecnica, Bologna, Italy, 14–16 May 1986, 171–184, 1986 (in Italian).

Cascini, L. and Versace, P.: Relationship between rainfall and landslide in a gneissic cover, in: Proceedings of the 5th International Symposium on Landslides, Lausanne, Switzerland, 565–570, 1988.

Cascini, L., Sorbino, G., Cuomo, S., and Ferlisi, S.: Seasonal effects of rainfall on the shallow pyroclastic deposits of the Campania region (southern Italy), Landslides, 11, 779–792, 2014.

CASMEZ: Carta Geologica della Calabria, F.229IIINE "Montalto Uffugo" (in scale 1:25000), Poligrafica & CarteValori, Ercolano, Napoli, Italy, 1967 (in Italian).

Cauvin, S., Cordier, M.-O., Dousson, C., Laborie, P., Lévy, F., Montmain, J., Porcheron, M., Servet, I., and Travé-Massuyès, L.: Monitoring and alarm interpretation in industrial environments, AI Commun., 11, 139–173, 1998.

Chow, V. T., Maidment, D. R., and Mays, L. W.: Applied Hydrology, Mc Graw Hill, New York, USA, 572 pp., 1988.

Corominas, J.: Landslides and climate, Keynote lecture, in: Proceedings of the 8th International Symposium on Landslides, vol. 4, Cardiff, United Kingdom, 26–30 June 2000, 1–33, 2000.

Crosta, G. B.: Regionalization of rainfall thresholds: an aid to landslide hazard evaluation, Environ. Geol., 35, 131–145, 1998.

Crosta, G. B., Dal Negro, P., and Frattini, P.: Soil slips and debris flows on terraced slopes, Nat. Hazards Earth Syst. Sci., 3, 31–42, doi:10.5194/nhess-3-31-2003, 2003.

Crozier, M. J.: The climate-landslide couple: a southern hemisphere perspective, in: Rapid mass movement as a source of climatic evidence for the Holocene, edited by: Matthews, J. A., Brunsden, D., Frenzel, B., Gläser, B., and Weiß, M. M., Gustav Fischer, Stuttgart, 333–354, 1997.

Cuomo, S. and Della Sala, M.: Rainfall-induced infiltration, runoff and failure in steep unsaturated shallow soil deposits, Eng. Geol., 162, 118–127, 2013.

D'Ambrosio, D., Spataro, W., and Iovine, G.: Parallel genetic algorithms for optimising cellular automata models of natural complex phenomena: an application to debris-flows, Comput. Geosci., 32, 861–875, 2006.

De Jong, K. A.: An analysis of the behavior of a class of genetic adaptive systems, PhD dissertation, Department of Computer and Communication Sciences, University of Michigan, Ann Arbor, USA, 1975.

Del Prete, M., Guadagno, F. M., and Hawkins, A. B.: Preliminary report on the landslides of 5 May 1998, Campania, southern Italy, Bull. Eng. Geol. Env., 57, 113–129, 1998.

Di Crescenzo, G. and Santo, A.: Analisi morfologica delle frane da scorrimento-colata rapida in depositi piroclastici della Penisola Sorrentina (Campania), Geogr. Fis. Dinam. Quat., 22, 57–72, 1999 (in Italian).

Di Crescenzo, G. and Santo, A.: Debris slides-rapid earth flows in the carbonate massifs of the Campania region (Southern Italy): morphological and morphometric data for evaluating triggering susceptibility, Geomorphology, 66, 255–276, 2005.

Dikau, R. and Schrott, L.: The temporal stability and activity of landslides in Europe with respect to climatic change (TESLEC): main objectives and results, Geomorphology, 30, 1–12, 1999.

Ducci, D. and Tranfaglia, G.: L'impatto dei cambiamenti climatici sulle risorse idriche sotterranee in Campania, Geologi. Boll. Ordine Geologi della Campania, 1–4, 13–21, 2005 (in Italian).

Ellen, S. D.: Description and mechanics of soil slip/debris flows in the storm, in: Landslides, floods, and marine effects of the storm of January 3–5, 1982, in the San Francisco Bay region, California, edited by: Ellen, S. D. and Wieczorek, G. F., U.S. Geol. Surv. Prof. Pap., 1434, 63–112, 1988.

Fienen, M. N., Doherty, J. E., Hunt, R. J., and Reeves, H. W.: Using prediction uncertainty analysis to design hydrologic monitoring networks: example applications from the Great Lakes water availability pilot project, US Geol. Surv., Reston Virginia, Scientific Investigations Report 2010-5159, 44 pp., 2010.

Fiorillo, F. and Wilson, R.: Rainfall induced debris flows in pyroclastic deposits, Campania (southern Italy), Eng. Geol., 75, 263–289, 2004.

Gariano, S. L., Brunetti, M. T., Iovine, G., Melillo, M., Peruccacci, S., Terranova, O., Vennari, C., and Guzzetti, F.: Calibration and validation of rainfall thresholds for shallow landslide forecasting in Sicily, southern Italy, Geomorphology, 228, 653–665, 2015.

Goldberg, D. E.: Genetic Algorithms in Search, Optimization and Machine Learning, Addison-Wesley, Boston, USA, 1989.

Gullà, G., Aceto, L., Antronico, L., Cilento, M., Niceforo, D., Perna, E., and Terranova, O.: Failure and post failure conditions of a landslide involving weathered and degraded rocks, in Proceedings of the IX International Symposium on Landslide, Rio de Janeiro, Brazil, 28 June-02 July 2004, 1241–1245, 2004.

Guzzetti, F.: Landslide fatalities and evaluation of landslide risk in Italy, Eng. Geol., 58, 89–107, 2000.

Guzzetti, F., Peruccacci, S., Rossi, M., and Stark, C. P.: Rainfall thresholds for the initiation of landslides in central and southern Europe, Meteorol. Atmos. Phys., 98, 239–267, 2007.

Guzzetti, F., Peruccacci, S., Rossi, M., and Stark, C. P.: The rainfall intensity-duration control of shallow landslides and debris flow: an update, Landslides, 5, 3–17, 2008.

Hinton, G. E. and Nowlan, S. J.: How learning can guide evolution, Complex Systems, 1, 495–502, 1987.

Holland, J. H.: Adaptation in Natural and Artificial Systems, University of Michigan Press, Ann Arbor, USA, 1975.

Hutchinson, J. N.: Deep-seated mass movements on slopes, Mem. Soc. Geol. It., 50, 147–164, 1995.

Iovine, G., D'Ambrosio, D., and Di Gregorio, S.: Applying genetic algorithms for calibrating a hexagonal cellular automata model for the simulation of debris flows characterised by strong inertial effects, Geomorphology, 66, 287–303, 2005.

Iovine, G., Iaquinta, P., and Terranova, O.: Emergency management of landslide risk during Autumn-Winter 2008/2009 in Calabria (Italy). The example of San Benedetto Ullano, in: Proceedings of the 18th World IMACS Congress and MODSIM09 International Congress on Modelling and Simulation , Modelling and Simulation Society of Australia and New Zealand and International Association for Mathematics and Computers in Simulation, July 2009, 2686–2693, 2009.

Iovine, G. G. R., Lollino, P., Gariano, S. L., and Terranova, O. G.: Coupling limit equilibrium analyses and real-time monitoring to refine a landslide surveillance system in Calabria (southern Italy), Nat. Hazards Earth Syst. Sci., 10, 2341–2354, doi:10.5194/nhess-10-2341-2010, 2010.

Jakob, M. and Weatherly, H.: A hydroclimatic threshold for landslide initiation on the North Shore Mountains of Vancouver, British Columbia, Geomorphology, 54, 137–156, 2003.

Keefer, D. K., Wilson, R. C., Mark, R. K., Brabb, E. E., Brown III, W. M., Ellen S. D., Harp, E. L., Wieczorek, G. F., Alger, C. S., and Zatkin, R. S.: Real-Time Landslide Warning During Heavy Rainfall, Science, 238, 921–925, 1987.

Köppen, W.: Climatologia, con un estudio de los climas de la tierra, Fondo de Cultura Economica, Mexico, 479 pp., 1948.

Krause, P., Boyle, D. P., and Bäse, F.: Comparison of different efficiency criteria for hydrological model assessment, Adv. Geosci., 5, 89–97, doi:10.5194/adgeo-5-89-2005, 2005.

Lanzafame, G. and Mercuri, T.: Interruzioni ferroviarie in Calabria conseguenti a fenomeni naturali (1950–1973), Geodata, 3, Cosenza, Italy, 46 pp., 1975 (in Italian).

Long, A. J.: RRAWFLOW: Rainfall-Response Aquifer and Watershed Flow Model (v1.15), Geosci. Model Dev., 8, 865–880, doi:10.5194/gmd-8-865-2015, 2015.

Marques R., Zêzere J., Trigo R., Gaspar J., and Trigo, I.: Rainfall patterns and critical values associated with landslides in Povoação County (São Miguel Island, Azores): relationships with the North Atlantic Oscillation, Hydrol. Process., 22, 478–494, 2008.

Mele, R. and Del Prete, S.: Lo studio della franosità storica come utile strumento per la valutazione della pericolosità da frane. Un esempio nell'area di Gragnano (Campania), Boll. Soc. Geol. Ital., 118, 91–111, 1999 (in Italian).

Mitchell, M.: An Introduction to Genetic Algorithms, MIT Press, Cambridge, United Kingdom, 1996.

Monaco, C. and Tortorici, L.: Active faulting in the Calabrian arc and eastern Sicily, J. Geodynam., 29, 407–424, 2000.

Montgomery, D. R. and Dietrich, W. E.: A physically-based model for the topographic control on shallow landsliding, Water Resour. Res., 30, 1153–1171, 1994.

Nolfi, S. and Marocco, D.: Evolving robots able to integrate sensory-motor information over time, Theor. Biosci., 120, 287–310, 2001.

Peres, D. J. and Cancelliere, A.: Derivation and evaluation of landslide-triggering thresholds by a Monte Carlo approach, Hydrol. Earth Syst. Sci., 18, 4913–4931, doi:10.5194/hess-18-4913-2014, 2014.

Petley, D. N.: The global occurrence of fatal landslides in 2007, in: International Conference on Management of Landslide Hazard in the Asia-Pacific Region, Tokyo, Japan, 590–600, 2008.

Pinault, J.-L., Plagnes, V., and Aquilina, L.: Inverse modeling of the hydrological and the hydrochemical behavior of hydrosystems: Characterization of karst system functioning, Water Resour. Res., 37, 2191–2204, 2001.

Pisani, G., Castelli, M., and Scavia, C.: Hydrogeological model and hydraulic behaviour of a large landslide in the Italian Western Alps, Nat. Hazards Earth Syst. Sci., 10, 2391–2406, doi:10.5194/nhess-10-2391-2010, 2010.

Poon, P. W. and Parks, G. T.: Optimizing PWR reload core design, Parallel Solving from Nature, 2, 371–380, 1992.

Pradhan, B. and Buchroithner, M.: Terrigenous Mass Movements: Detection, Modelling, Early Warning and Mitigation Using Geoinformation Technology, Springer, 400 pp., 2012.

Rossi, F. and Villani, P. (Eds.): Valutazione delle piene in Campania, CNR-GNDCI publications, Grafica Metellioana &C., Cava de' Tirreni, Italy, 310 pp., 1994.

Salvati, P., Bianchi, C., Rossi, M., and Guzzetti, F.: Societal landslide and flood risk in Italy, Nat. Hazards Earth Syst. Sci., 10, 465–483, doi:10.5194/nhess-10-465-2010, 2010.

Sengupta, A., Gupta, S., and Anbarasu, K.: Rainfall thresholds for the initiation of landslide at Lanta Khola in north Sikkim, India, Nat. Hazards, 52, 31–42, 2010.

Servizio Geologico, Sismico dei Suoli: I numeri delle frane, Regione Emilia-Romagna Publisher, Bologna, 94 pp., 1999 (in Italian).

Servizio Idrografico: Annali Idrologici, Parte I, Compartimento di Napoli, Istituto poligrafico e Zecca dello Stato, Rome, Italy, 1948–1999.

Sirangelo, B. and Versace, P.: A real time forecasting for landslides triggered by rainfall, Meccanica, 31, 1–13, 1996.

Sorriso-Valvo, G. M., Agnesi, V., Gulla, G., Merenda, L., Antronico, L., Di Maggio, C., Filice, E., Petrucci, O., and Tansi, C.: Temporal and spatial occurrence of landsliding and correlation with precipitation time series in Montalto Uffugo (Calabria) and Imera (Sicilia) areas, in: Temporal occurrence and forecasting of landslides in the European Community, Final Report, II, European Community, Programme EPOCH, Contract 90 0025, edited: by Casale, R., Fantechi, R., and Flageollet, J. C., 825–869, 1994.

Sorriso-Valvo, G. M., Antronico, L., Catalano, E., Gullà, G., Tansi, C., Dramis, F., Ferrucci, F., and Fantucci, R.: Final Report (June 1996), CNR-IRPI, in: The temporal stability and activity of landslides in Europe with respect to climatic change (TESLEC), Final Report, Part II, edited by: Dikau, R., Schrot, L., Dehn, M., Hennrich, K., and Rasemann, S., 87–152, 1996.

Terlien, M. T. J.: The determination of statistical and deterministic hydrological landslide-triggering thresholds, Environ. Geol., 35, 125–130, 1998.

Terranova, O.: Caratteristiche degli eventi pluviometrici a scala giornaliera in Calabria, in: XXIX Convegno di Idraulica e Costruzioni Idrauliche, Trento, Italy, 07–10 September 2004, 343–350, 2004 (in Italian).

Terranova, O., Antronico, L., and Gullà, G.: Pluviometrical events and slope stability on weathered and degraded rocks (Acri, Calabria, Italy), in Proceedings of the IX International Symposium on Landslide, Rio de Janeiro, Brazil, 28 June–02 July 2004, 335–342, 2004.

Terranova, O., Iaquinta, P., Gariano, S. L., Greco, R., and Iovine, G.: ^{CM}*SAKe*: A hydrological model to forecasting landslide activations, in: Landslide Science and Practice, vol. 3, edited by: Margottini, C., Canuti, P., and Sassa K., Springer, 73–79, 2013.

Terzaghi, K.: Stability of steep slopes on hard unweathered rock, Geotechnique, 12, 251–270, 1962.

Trigila, A.: Rapporto sulle frane in Italia. Il Progetto IFFI. Metodologia, risultati e rapporti regionali, APAT, Roma, Italy, 681 pp., 2007 (in Italian).

Trigo, R. M., Zêzere, J. L., Rodrigues, M. L., and Trigo, I. F.: The influence of the North Atlantic Oscillation on rainfall triggering of Landslides near Lisbon, Nat. Hazards, 36, 331–354, 2005.

UNDRO: Mitigating Natural Disasters. Phenomena, Effects and Options, United Nations, New York, USA, 164 pp., 1991.

Van Asch, Th. V. J., Buma, J., and Van Beek, L. P. H.: A view on some hydrological triggering systems in landslides, Geomorphology, 30, 25–32, 1999.

Vennari, C., Gariano, S. L., Antronico, L., Brunetti, M. T., Iovine, G., Peruccacci, S., Terranova, O., and Guzzetti, F.: Rainfall thresholds for shallow landslide occurrence in Calabria, southern Italy, Nat. Hazards Earth Syst. Sci., 14, 317–330, doi:10.5194/nhess-14-317-2014, 2014.

White, I. D., Mottershead, D. N., and Harrison, J. J.: Environmental Systems, 2nd Edn., Chapman & Hall, London, United Kongdom, 616 pp., 1996.

Wieczorek, G. F.: Effect of rainfall intensity and duration on debris flows in central Santa Cruz Mountains, California, in: Debris Flows/Avalanches: Processes, Recognition and Mitigation, edited by: Costa, J. E. and Wieczorek G. F., Geological Society of America, Reviews in Engineering Geology 7, 93–104, 1987.

Wieczorek, G. F. and Glade, T.: Climatic factors influencing occurrence of debris flows, in: Debris flow hazards and related phenomena, edited by: Jakob, M. and Hungr, O., Berlin Heidelberg, Springer, 325–362, 2005.

Wilson, R. C. and Wieczorek, G. F.: Rainfall thresholds for the initiation of debris flow at La Honda, California, Environ. Eng. Geosci., 1, 11–27, 1995.

Zêzere, J. L. and Rodrigues, M. L.: Rainfall thresholds for landsliding in Lisbon area (Portugal), in Landslides, edited by: Rybar, J., Stemberk, J., and Wagner, P., A.A. Balkema, Lisse, The Netherlands, 333–338, 2002.